Project Report

University Grants Commission Sponsored

Major Research Project

[File No. 42-788/2013 (SR)]

[01 April 2013 to 31 March 2017]

Morphological and Relative Humidity/Gas Sensing Studies of Undoped and Doped Nanomaterials

Principal Investigator

Prof. N. K. Pandey

Department of Physics, University of Lucknow
Lucknow-226007, Uttar Pradesh, India.
E-mail: profnarendrapandey137@gmail.com

Acknowledgements

I am thankful to the University Grants Commission for providing the financial support for the project. Iam also thankful to the University of Lucknow for allowing me to carry on with the project work. I should be thankful to the registrar and staff of the registrar office; and finance officer and his staff for facilitation of the paper and other works. My thanks are also due for the Department of Physics, University of Lucknow for providing the infrastructural facilities for carrying out the project work. Iwill be failing in the acknowledge if I do not thank my students Dr. Suneet Kumar Misra, Dr. (Mrs) VandnaShakya, Dr. Anoop Kumar Gautam, Dr. (Miss)Vijay Bharti Rajput, Dr.Abhishek Panwar and Mr. VikasVermafor carrying on with different parts of the project work.

My thanks are also due for the Geological Survey of India, Lucknow for providing the XRD and Scanning Electron Microscope studies of the samples. I also thank the BirbalSahni Institute of Paleobotany, Lucknow for providing the Scanning Electron Microscope studies of the samples.

I am thankful to the chemical suppliers Sabina Scientific Corporation, Lucknow; Mullik Biological House, Lucknow and National Scientific Suppliers, Lucknow for providing the required chemicals and glass wares in time.

I am thankful to my wife Shobha, my daughters Harsha and Varsha for having patience and allowing me to have time away from the family to complete the project.

At the outset, I am thankful to all those people who have been of any help to me in the facilitation of the project directly or indirectly.

Prof. N. K. Pandey

Principal Investigator

Contents

CHAPTER V

V_2O_5-ZnO Nanocomposite for Moisture Sensing Studies

CHAPTER VI

Application of Undoped and Al_2O_3 doped ZnO Nanomaterials as a Solid-State Humidity Sensor and its Characterization Studies

CHAPTER VII

Nanostructured Undoped and Cu-doped ZnO Thin Films as Gas Sensor

CHAPTER VIII

Nanostructured Zinc Oxide Prepared through Solid State Reaction Route as Gas Sensor

CHAPTER I

Moisture Sensing Studies of CuO-ZnO Nanocomposites Prepared by Solid State Reaction Method

Here, the CuO-ZnO nanocomposite samples with different weight % (0.2, 0.4, 0.6, 0.8 and 1) of CuO were successfully prepared through solid-state reaction route. The pellet samples were made under a pressure of 390 M Pascal and room temperature. Prepared pellet samples were annealed at 400°C temperature for 4 hours in a muffle furnace. The electrical resistance of nanocomposites continuously decreased when relative humidity (RH) was increased from 10% to 95% RH. SEM and XRD of the sensing element have been studied.

1.1 Introduction

Humidity is an essential constituent of our environment and it plays a very important role in human life. Research has been going on to find out suitable material that show good sensitivity over a large range of relative humidity (RH) low hysteresis and ageing effect. Among semiconductor metal oxides n-type Zinc Oxide (ZnO) is a versatile semiconductor material having excellent electronic and optic properties [1-6]. For humidity sensing point of view, the morphology (e.g diameter of nanoparticles), stoichiometry (e.g oxygen vacancy) as well as composition (e.g dopants), all have significant influences on their humidity sensing properties [7-10].

The interest in ZnO structures has increased drastically in recent years. Zinc oxide is an inorganic compound with the formula ZnO. It is a white powder that is insoluble in water. The mineral form of ZnO takes up a red or yellow colour instead of the usual white due to the presence of impurities like Manganese and other elements. Crystalline form of ZnO is thermochromic in nature and due to this it changes from white to yellow on heating and vice versa on cooling. ZnO is a wide-band gap semiconductor of the II-VI semiconductor group (since oxygen was an element of VIA group and zinc is IIB) of the periodic table. Zinc oxide is widely used as an additive in numerous materials and products including glass, rubbers, plastics, ceramics, cement, lubricants ointments, adhesives, sealants, pigments, foods, batteries, ferrites, fire retardants, paints and first-aid tapes. It occurs naturally as the mineral zincite, but most zinc oxide is produced synthetically. ZnO is a versatile functional material having direct wide band gap (3.37 eV) semiconductor with a high thermal and chemical stability, resistivity control over the range 10^{-3}– 10^{5} Ωcm, good electrical and optical property, suitability to doping, non-toxicity, low cost, transparency in the visible range, high electron mobility, and abundance in nature. It has shown promising application at nanoscale. Those properties are used in emerging applications for transparent electrodes in liquid crystal displays, in energy-saving or heat-protecting windows, and in electronics as thin-film transistors and light-emitting diodes. As a wide direct bandgap, II-VI semiconductor, zinc oxide (ZnO) has a large exciton binding energy of 60 mV with a hexagonal wurtzite structure (a = 3.249 Å and c = 5.21 Å) [11-30].

ZnO has received much attention over the past few years because it has a wide range of properties that depend on doping, including a range of conductivity from metallic to insulating (including *n*-type and *p*-type conductivity), high transparency, piezoelectricity, wide-band gap semiconductivity, room-temperature ferromagnetism, and huge magneto optic and chemical-sensing effects. Without

much effort, it can be grown in many different nanoscale forms, thus allowing various novel devices to be achieved.Zno is an ideal candidate for applications like transparent conducting electrodes in flat panel displays and window layers in solar cells [31-33]. ZnO nanostructures have an active role to play in nano devices like nano gas sensors because the huge surface area enhances the gas sensing properties of the sensors. Apart from this, bio-safe characteristics of ZnO make it very attractive for biomedical applications. [34-36]. ZnO is a compound semiconductor whose 'ionicity' resides at the borderline between the covalent and ionic semiconductors. Its elastic constants are not that impressive but ZnO has got very good thermal properties like high melting point, high thermal capacity and conductivity and a low coefficient of thermal expansion which makes it suitable for use as a humidity sensor [37-44].

ZnO has three crystal forms: the hexagonal wurtzite, the cubic zinc blende and the cubic rock salt which is rarely observed. The hexagonal wurtzite structure is most commonly used as it has the highest stability at room temperature. Hexagonal and zinc blende structures don't display inversion symmetry and it is properties like these that are responsible for the piezoelectricity and pyroelectricity of ZnO. The zinc-blende structure can be stabilized only by the growth on cubic structure while rock salt (NaCl) structure may be obtained at relatively high pressure. ZnO is considered to be a soft material with a reading of 4.5 on the Mohs hardness scale.

Due to its unique properties like wide band gap and large excitation binding energy, ZnO has the potential to be applied as chemical sensors, solar cells, luminescence devices etc. The fundamental study of the electrical properties of ZnO nanostructures is crucial for developing their future applications in nanoelectronics. Electrical transport measurements have been performed on individual ZnO nanowires and nanorods. ZnO nanowires are also reported to have behaved like a n-type semiconductor due to the presence of interstitial defects and vacancies. P-type and n-type ZnO nanowires can serve as p-n junction diodes and LEDs. Field effect transistors (FETs) fabricated from them can be used to make complementary logic circuits [45-62].

Doping is an effective technique for manipulating various applications of semiconductors. Copper is a chemical element, having atomic number 29. It is a ductile metal with very high thermal and electrical conductivity. Pure copper is soft and malleable; a freshly exposed surface has a reddish-orange color. It is used as a conductor of heat and electricity, a building material, and a constituent of various metal alloys. Copper forms a rich variety of compounds, usually with oxidation states +1 and +2, which are often called cuprous and cupric, respectively. Copper compounds are known in several oxidation states, usually 2^{+}, where they often impart blue or green colors to natural minerals such as turquoise and have been used historically widely as pigments. Copper as both metal and pigmented salt, has a significant presence in decorative art. Copper 2^{+} ions are soluble in water, where they function at low concentration as bacteriostatic substances and fungicides. For this reason, copper metal can be used as an antigerm surface that can add to the anti-bacterial and antimicrobial features of building such as hospital. Copper is 100% recyclable without any loss of quality, regardless of whether it is in a raw state or contained in a manufactured product.In sufficient amount, copper salts can be poisonous to higher organisms. However, despite universal toxicity at high concentration, the 2^{+} copper ions at lower concentration is an essential trace nutrient to all higher plant and animal life. In animals, including humans, it is found widely in

tissues, with concentration in liver, muscle, and bone. Copper compounds are used as bacteriostatic substances, fungicides, and wood preservatives.

Copper forms two well-known stable oxides, cupric oxide (CuO) and cuprous oxide (Cu_2O). These two oxides have different physical properties, different colors, crystal structures andelectrical properties. Cu,as a group Ib element (Cu, Ag and Au), can assume a valency of either +1 or +2 depending on its chemical configuration, for example in the compounds Cu_2O and CuO, respectively. The radii of Cu^+ (98 pm) and Cu^{2+} (80 pm) ions are similar to that of Zn^{2+} ion (83 pm), compared with that of Ag^+ ion (113 pm) in the same Ib group. The possibility of low cost production methods and the good electrochemical properties make CuO to be one of the best materials for electrical, optical, sensing and so forth. However, copper oxide is a semiconductor with a band gap of 1.4 ev, which absorbs strongly in a visible spectrum [63-64].

If Cu is needed to become an acceptor upon the substitution at a Zn site, it will have to assume a valency of +1 [24]. It is known that group Ib metals are fast-diffusing in compound semiconductors. The diffusion of Cu into ZnO can cause the formation of complex centres (Cu_{Zn}, Cu_i). It is possible that Cu atoms can replace either substitutional or interstitial Zn atoms in the ZnO lattice creating structural deformations [65].
Many studies have focused on the change of physical properties when Cu was induced into ZnO [66]. A potential *p*-type doping candidate CuO has been chosen for ZnO [67]. The copper oxide (CuO) is a narrow band gap (1.7 eV) p-type semiconductor material having monoclinic crystal structure[68] and draw much attention since the starting growth material is inexpensive and easy to get, and the methods to prepare these materials are of low cost [69]. The hetero nanocomposites of p-type CuO and n-type ZnO semiconductor have been reported to enhance the electron-hole separation [70]. In general, combination of narrow band gap semiconductors with wide band gap semiconductors will increase their sensing property [71-74]. These nanocomposites are already used in several applications such as solar cells [75], gas sensors [76], biosensors [77], and humidity sensors [78]. These reported nanocomposite materials also showed various nanostructural morphologies, for examples, nano-rings, nano-combs, nano-belts, nano-tubes, nano-rods and nano-sheets [79]. Other reasons for choosing copper oxide as an addition to ZnO is that the behavior of Cu was found as an acceptor impurity in n-type ZnO and it had a significant effect on the electrical and optical properties of ZnO [80-83]. CH. Ashok and K. Venkateswara Rao et al. [84] reported that the humidity sensitivity of the nanocomposite ZnO/CuO synthesized by microwave-assisted technique has been increased along with increasing of annealing temperature. Some researchers have reported the varistor properties of polycrystalline ZnO:Cu [85]. Qi Qi et al. [86] have studied the humidity sensing application of KCl-doped Cu–Zn/CuO–ZnO nanoparticles in the range of 11–95% RH and reported the two orders of magnitude change in impedance and the response and recovery time of about 40-50s. The maximum hysteresis was found to around 4% RH. Investigations were also carried out by Jeseentharani et al. [87] for analyzing humidity sensing properties of the composites prepared by mixing 1:1 mole ratio of CuO-ZnO, CuO-NiO, and NiO-ZnO compounds sintered at 800°C for 5 h in the range of 5%–98% RH. It was noticed that CuO-NiO compound possessed the best humidity sensitivity. The response and recovery times of the CuO-NiO composites were 80 and 650 s, respectively. Pandey et al. [88-90] have studied moisture sensing application of Cu_2O-doped ZnO nanocomposite and Ag-WO_3 and TiO_2-ZnO nanocomposites. They showed that best results with sensitivity of 4.78 MΩ/%RH for the nanocomposite with 20% of Cu_2O doped ZnO annealed at

temperature of 400ºC. In the case of Ag-WO_3 they got the best result with sensitivity of 2.38 MΩ/%RH and in the case of TiO_2-ZnO, the sensitivity 9.08 MΩ/%RH was achieved. In this chapter we report the characterization and humidity sensing studies of CuO-ZnO nanomaterials prepared by solid state reaction route. In the present case, the reproducibility has been found very high, the effect of ageing and hysteresis low as compared to the earlier cases. In the present work, the sample CuO-ZnO nanocomposite showed the best results with sensitivity 110% higher than Ag-WO_3 nanocomposite, 230% higher than that of TiO_2-ZnO nanocomposite and 526% higher than Cu_2O-ZnO nanocomposite. Doping and annealing Temperature affects various significant properties, morphologies and crystalline nature of pure and doped ZnO nanocomposite.

1.2 Fabrication of Sensing Elements

CuO-ZnO nanocomposite samples with different weight % (0.2, 0.4, 0.6, 0.8 and 1) of CuO were successfully prepared through solid-state reaction route. Pure Zinc oxide (MERC, India Ltd), and copper oxide (MERC, India Ltd) of different wt% and 10% of glass powder (binder) by weight were thoroughly mixed and ground with the help of agate mortar and pestle. The uniformly and homogeneously mixed powders were pressed at room temperature into disc shaped pellets (thickness of 3mm and diameter of 12 mm) under a pressure of 390 M Pascal in a hydraulic press. Prepared pellet samples of pure ZnO, CZ-0.2 (0.2% by weight of CuO in ZnO), CZ-0.4 (0.4% by weight of CuO in ZnO), CZ-0.6 (0.6% by weight of CuO in ZnO), CZ-0.8 (0.8% by weight of CuO in ZnO), and sample CZ-1(1.0% by weight of CuO in ZnO), were annealed in air at 400°C for 4 hours in a muffle furnace. Now, the experiment was performed in the humidity chamber as shown in Figure 1.1.

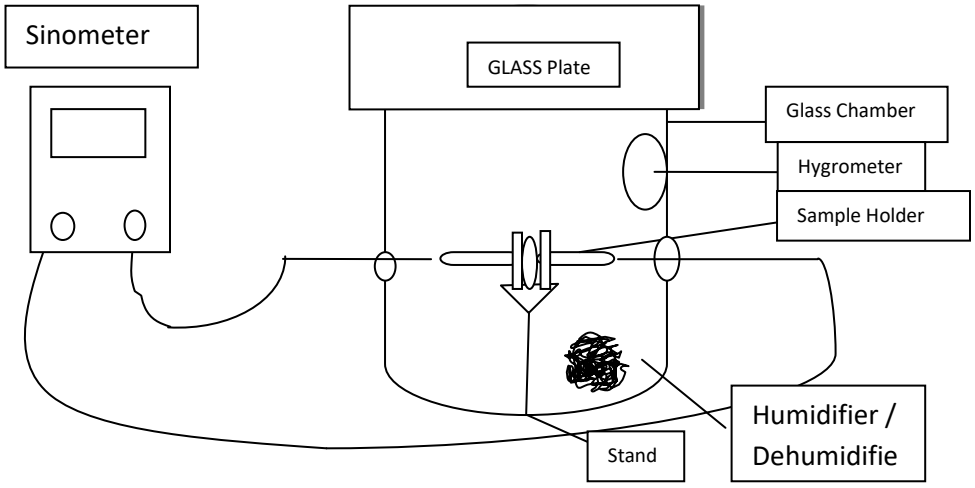

Figure 1.1 Schematic arrangement of humidity sensing apparatus

1.3 Scanning Electron Microscope (SEM) Studies

The surface morphology of the pellet samples were investigated through scanning electron microscope (JEOL 7610F Japan) with an accelerating voltage of 5 kV at a magnification of 3,000 KX. The surfaces of the pellets were coated with 10 nm thick films of gold metal by DC sputtering

before SEM observation. SEM of the sample CZ-1. SEM micrographs would reveal porous structure and small crystallites without inside pores but many inter grain pores. Higher porosity increases surface to volume ratio of the materials and therefore, helps in getting good sensitivity. The average grain size calculated from SEM micrographs, for CZ-1 is 200 nm while for the sample of pure ZnO it is 250 nm annealed at 400°C. Figures 1.2 and 1.3 are SEM micrographs.

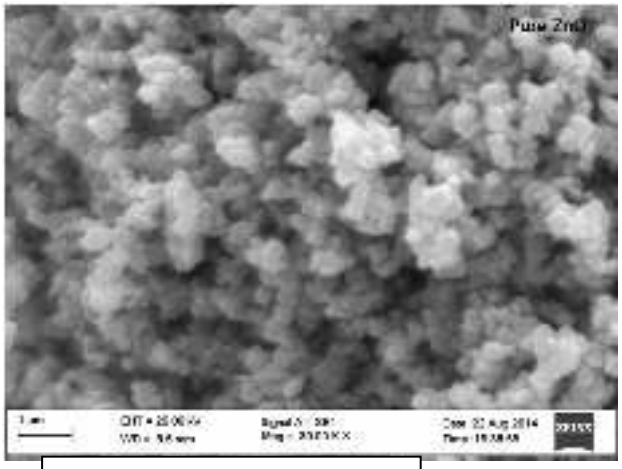

Figure 1.2 SEM of pure ZnO

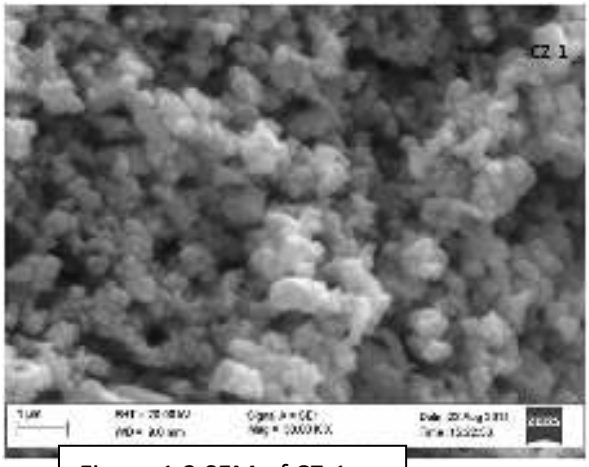

Figure 1.3 SEM of CZ-1

1.4 X-Ray Diffraction Studies

Figure 1.4 shows the X-ray diffraction (XRD) patterns for the sensing elements of CZ-1 annealed at temperature 400°C. Tables 3.6 representsone XRD peak positions, d-spacing and miller indices for sample of CZ-1. The d-spacing values of pure ZnO and CuO-ZnO nanocomposite from JCPDS cards are almost equal to measured d-spacing values from Bragg's law. The average crystalline size of the samples was calculated using Debye-Scherer's formula [61-62] and Williamson and Hall (W-H) method [63]. Debye Scherer's formula is given by the following expression:

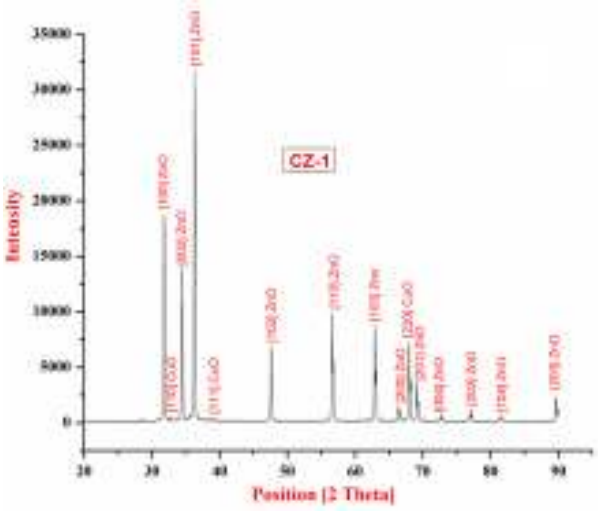

Figure 1.4 XRD patterns for CZ-1

$$\textbf{Crystallite Size}(\mathbf{D}) = \frac{\mathbf{0.9\lambda}}{\boldsymbol{\beta}\mathbf{Cos}\boldsymbol{\theta}} \qquad \text{……..(1)}$$

Where $\boldsymbol{\lambda}$ is the wavelength of the X-ray used and β is the full width at half maxima (FWHM).
The broadening of x-ray diffraction peaks are caused by decreasing crystallite-size and by strain associated with lattice distortions due to lattice defects. Williamson and Hall proposed that peak broadening profiles due to both size and strain are Lorentzian. Based on this, they derive a relation between average crystallite size (D) and the lattice microstrain (ε) as follows:

$$\boldsymbol{\beta}\mathbf{cos}\boldsymbol{\theta} = \mathbf{k}\boldsymbol{\lambda}/\mathbf{D} + 4\boldsymbol{\varepsilon}\,\mathbf{sin}\boldsymbol{\theta} \qquad \text{……(2)}$$

Where $\boldsymbol{\beta}$ is full width half maxima, $\boldsymbol{\lambda}$ is the wavelength of the radiation (1.54060 *A* for *CuKα* radiation), $\boldsymbol{k}$ is a constant equal to 0.94, and $\boldsymbol{\theta}$ is the peak position. A plot of $\boldsymbol{\beta}\mathbf{cos\theta}$ versus $\mathbf{4}\boldsymbol{sin\theta}$results in a straight line and the values for crystallite size (**D**) and lattice strain ($\boldsymbol{\varepsilon}$) can then be obtained from the intercept and the slope of the straight line, respectively. Figure 1.5 shows one such Williamson and Hall plot for CZ-1. The crystallite size calculated from using Debye-Scherer's formula and W-H plots for pure ZnO, CZ-0.2, CZ-0.4, CZ-0.6, CZ-0.8 and CZ-1 are presented in Table 1.1.

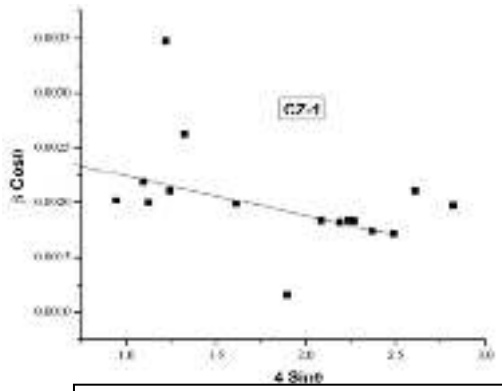

Figure 1.5 Williamson and Hall plot for CZ-1

1.5 Results and Discussion

Variation in resistance with change in relative humidity for all the sensing elements viz. pure ZnO, CZ-0.2, CZ-0.4, CZ-0.6, CZ-0.8 and CZ-1 is shown in Figure 1.6. Secular decrease in the value of resistance with increase in the % RH was recorded for all samples under investigation. Samples CZ-0.8 and CZ-1 exhibited higher values of resistance and sharp decline in the value of resistance as compared to sensing elements pure ZnO, CZ-0.2, CZ-0.4 and CZ-0.6 up to relative humidity 35% RH. After 35% RH, all the sensing elements i.e. pure ZnO, CZ-0.2, CZ-0.4, CZ-0.6, CZ-0.8 and CZ-1 showed the similar trend in the variation of resistance with RH. The decrease in the resistivity of the sample with relative humidity in the lower range may be suspected due to the adsorption of the water molecules on the pellet surface with capillary nanopores. The semiconductor humidity sensor usually works on the principle of amount of water adsorption on the pellet surface. Adsorption of moisture affects the proton conduction on the surface and the conductivity varies with amount of water adsorbed by it. This principle is employed for the measurement of humidity in resistive type humidity sensor. Higher porosity increases surface to volume ratio of the material and enhances diffusion rate of water into or out of the porous structure and thus helps in getting good sensitivity. At high relative humidity, liquid water condenses in the capillary like pores, forming a liquid like layer.

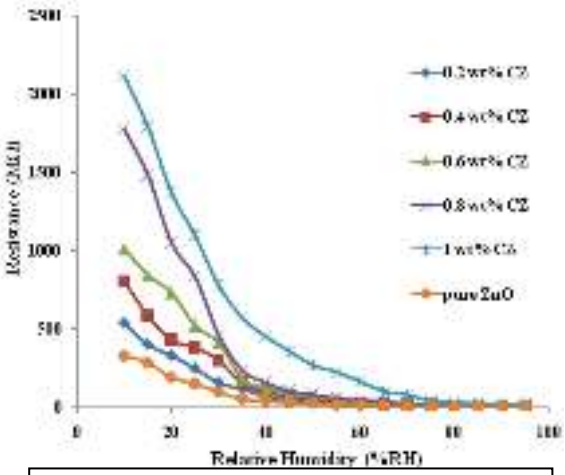

Figure 1.6 Resistance Vs Relative Humidity

Figure 1.7 Sensitivity Vs Dopant %

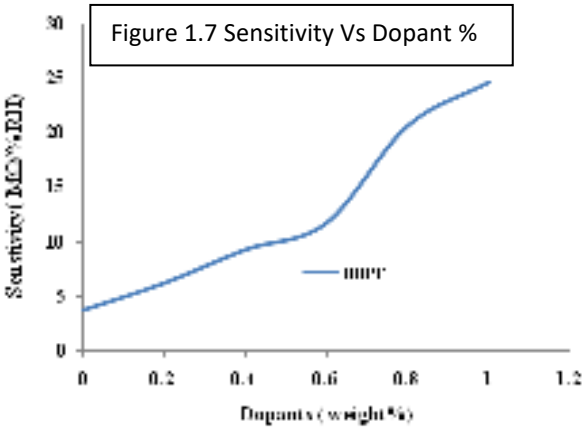

The hysteresis effect is due to initial chemisorptions on the surface of the sensing elements. The chemisorbed layer once formed is not further affected by exposure to or removal of humidity, it can be thermally desorbed only. Hence in the decreasing

cycle of % RH the initial adsorbed water is not fully removed leading to hysteresis. The results were generally found to be reproducible over different cycles of operation.
After humidity treatment the sensing element samples was kept in laboratory environment and its humidity sensing characteristic was regularly monitored after three months. To see the effects of aging and reproduction the sensing elements have again been then exposed to humidity after three months. The results have been found to be generally reproducible over different cycles of operation.

All the sensing elements generally show increase in sensitivity with increase in percentage of CuO in ZnO for annealing temperature 400°C. The sensitivity for the samples of pure ZnO, CZ-0.2, CZ-0.4, CZ-0.6, CZ-0.8, and CZ-1 have been calculated and shown in Table 1.4. All the sensing elements show increase in sensitivity with increase in weight percentage of CuO in ZnO. The sample CZ-1 shows maximum sensitivity of 29.95 MΩ /%RH among all the samples. Above 1 weight % of CuO addition in ZnO, though the sensitivity increased however, the higher aging and higher hysteresis were also observed. Figure 1.7 shows the variation of sensitivity with weight % of CuO in ZnO.

As reported in the table 1.2, the average crystallite size for the samples of pure ZnO, CZ- 0.2, CZ- 0.4, CZ- 0.6, CZ- 0.8 and CZ-1 calculated using Debye-Scherer's formula were found to be 79.30 nm, 77.43 nm, 76.29 nm, 74.86 nm, 71.08 nm and 70.55 nm respectively and the crystallite size calculated from W-H plot for the samples of pure ZnO, CZ- 0.2, CZ- 0.4, CZ- 0.6, CZ- 0.8 and CZ-1 was found to be 81 nm, 79.68 nm, 78.97 nm, 68.44 nm, 67.98 nm, 66.95 nm respectively. From both the methods, thus, with increase in the doping % of CuO in ZnO, the crystallite size decreases. This led to the increase in the surface to volume ratio. Thus, with increase in weight % of additives, more of the surface area of the samples was getting exposed for adsorption, leading to increase in sensitivity.

Table 1.1 X-ray diffraction peak position, d-spacing and Miller indices for CZ-1.0 sample.

S. No.	Samples	Crystallite size (nm)	
		From Scherer's formula	From W-H Graph
1	Pure ZnO	79.30	81
2	CZ-0.2	77.43	79.68
3	CZ-0.4	76.29	78.97
4	CZ-0.6	74.86	68.44
5	CZ-0.8	71.08	67.98
6	CZ-1	70.55	66.95

Table 1.2 Crystallite size (nm) calculated from the observed x-ray diffraction patterns for the pure ZnO and CuO-ZnO nanocomposite samples.

S. No.	Position [degree]	Compound		d-spacing [from JCPDS] (Å)	d-spacing [By Bragg's Law] (Å)	Miller Indices
		ZnO	CuO			
1	31.832	√		2.815	2.8089	(100)
2	32.717		√	2.751	2.7349	(110)
3	34.488	√		2.602	2.5984	(002)
4	35.59		√	2.523	2.521	(-111)
5	36.319	√		2.476	2.47152	(101)
6	38.75		√	2.323	2.3221	(111)
7	47.600	√		1.910	1.90878	(102)
8	56.6464	√		1.625	1.62354	(110)
9	62.9122	√		1.476	1.47607	(103)
10	66.420	√		1.407	1.40636	(200)
11	68.000		√	1.375	1.37748	(220)
12	69.138	√		1.358	1.35756	(201)
13	72.624	√		1.301	1.30076	(004)
14	77.004	√		1.238	1.23731	(202)
15	81.424	√		1.181	1.18095	(104)
16	89.667	√		1.093	1.09253	(203)

Table 1.3 Crystallite size (D) calculated for different peaks with corresponding 2θ and FWHM values for sample CZ-1 annealed at 400°C.

2θ	FWHM (β) (deg)	Crystallite size (D) (nm)
31.832	0.131	66.1
32.717	0.120	72.1
34.488	0.122	71.0
35.59	0.21	41.6
36.319	0.128	68.1
38.75	0.16	56.1
47.6	0.125	72.8
56.646	0.119	78.6
62.912	0.124	78.4
66.42	0.125	79.4
68.0	0.128	78.0
69.138	0.128	79.0
72.624	0.124	83.1
77.004	0.143	74.2
81.424	0.160	68.5
89.667	0.160	73.2

Table 1.4 Sensitivity (MΩ/%RH) of pure ZnO and CuO-ZnO nanocomposite samples.

Samples	Sensitivity of Samples (MΩ /%RH) over the entire range from 10 to 95 % RH for annealing temperature 400°C		
	a	b	c
Sample Pure ZnO	3.76	4.21	3.42
Sample CZ-0.2	6.23	7.07	5.88
Sample CZ-0.4	9.30	11.38	8.54
Sample CZ-0.6	11.74	13.83	11.14
Sample CZ-0.8	20.64	24.50	19.17
Sample CZ-1	24.70	29.95	21.80

[a]Increasing Cycle of Relative Humidity; [b]Decreasing Cycle of Relative Humidity; [c]Increasing Cycle after three months.

References

1. B. C. Yadav, R. Srivastava, C. D. Dwivedi and P. Pramanik, "Moisture sensor based on ZnO nanomaterial synthesized through oxalate route" , Sensors and Actuators, B 131 216–222 (2008).
2. Shobhna Dixit, Anchal Srivastava, R.K.Shukla, Atul Srivastava, "Pulsed laser deposited ZnO films and their humidity sensing behavior", J Mater Science: 19 788-792 (2008).
3. Nguyen Le Hung, "Synthesis and Gas Sensing Properties of ZnO Nanostructures", Journal of the Korean Physical Society, 57 1784-1788 (2010).
4. Z. Chen, M. C. Jin and C. Zhen, "Humidity sensors with reactively evaporated Al2O3 films as porous dielectrics" Sensors and Actuators B, 2 167-17 (1990).
5. N.K.Pandey, K.Tiwari and Akash Roy,"ZnO:TiO2 nanocomposite: Characterization and moisture sensing sttudies" Bull.Mater.Sci., 35 347-352 (2012).
6. P.M.Faia and C.S.Furtado, "Effects of composition on electrical response to humidity of TiO2 : ZnO sensors investigated by impedance spectroscopy", Sensors and ActuatorsB, 181 720-729 (2013).
7. I. Petrila and F. Tadorache, "Humidity sensor applicative material based on copper-zinc-tungsten spinel ferrite", Mater. Lett., 108 129-133 (2013).
8. N.K.Pandey, Karunesh Tiwari and Akash Roy, "Moisture Sensing Application of Cu_2O Doped ZnO Nanocomposites", IEEE Sensors Journal, 11 9 (2011).
9. Prashant S Vachhani, Giusepe Dalba, Raj Kumar Ramamoorthy, Francesco Rocca, Ondrej Sipr and Anil K Bhatnagar, "Cu doped ZnO pellets: study of structure and Cu specific magnetic properties", J. Phys.: Condens. Matter, 24 506001 (2012).
10. Indra Bahadur Karki, Jeevan Jyoti Nakarmi and Suman Chatterjee, "Synthesis of Zinc oxide Nanorods and its Application to Humidity Sensor", Journal of Institute of Science and Technology, 20 36-39 (2015).
11. P.S. Gupta, Nanda Shakti, "Structural and Optical Properties of Sol-gel Prepared ZnO Thin Film" Applied Physics Research, 2 19-28 (2010).
12. P. Raji, H. S. Binitha,and K. Balachandra Kumar "Synthesis and Humidity Sensing Properties of Sn-Doped Nano-TiO_2", Journal of Nanotechnology, 2011 1-6 (2011).
13. Richa Srivastava, "Investigation on Temperature Sensing of Nanostructured Zinc Oxide Synthesized via Oxalate Route", Journal of Sensor Technology, 2 8-12 (2012).
14. K. C. Dubey, Abhay S. Jaiswal and R. K. Shukla, "Synthesis, Optical and Humidity Sensing properties of pure ZnO and ZNO: SNO_2 thin films", International Journal of Research in Engineering & Technology, 3 57-62 (2015).
15. L. C. Nehru, M. Umadevi, C. Sanjeeviraja, "Studies on Structural, Optical and Electrical Properties of ZnO Thin Films Prepared by the Spray Pyrolysis Method", International Journal of Materials Engineering, 2 12-17 (2012).
16. A Ghosh, N Kumari, S Tewari, A Bhattacharjee, "Structural and optical properties of pure and Al doped ZnO nanocrystals", Indian Journal of Physics, 87 1099-1104 (2013).
17. Richa Srivastava, "Investigation on Temperature Sensing of Nanostructured Zinc Oxide Synthesized via Oxalate Route", Journal of Sensor Technology, 2 8-12 (2012).
18. Qi Qi, Tong Zhanga,, Yi Zenga, Haibin Yang, "Humidity sensing properties of KCl-doped Cu–Zn/CuO–ZnO nanoparticles" , Sensors and Actuators B, 137 21–26 (2009).
19. Barnaby J. Feder (March 26, 2008). "Regulators Stamp Copper as a Germ Killer". New, York Times. http//www.nytimes.com /2008/03/26/ business/ 26microbes. html_r=1 & cp=2 &sq=copper &st=ny&oref=slogin.
20. Brown, Lester (2006). Plan B 2.0: Rescuing a Plant Under Stress and a civilization in Trouble. New York: w.w.Norton. p.109. ISBN 0393328317.
21. A. C. Saritha, M. R. Shijeesh, L. S. Vikas, Rajeev R. Prabhu and M K Jayaraj, "Growth and characterization of p-ZnO:Cu thin film and its homojunction application",Journal of Physics D: Applied Physics, 49 29 (2016).
22. Chih-Hung Hsu, Lung-Chien Chen and Xiuyu Zhang, "Effect of the Cu Source on Optical Properties of Cu-ZnO Films Deposited by Ultrasonic Spraying", Materials, 7 1261-1270 (2014).
23. J. Ghijsen, L.H Tjeng, J. van Elp, H. Eskes, J. Westerink, and G.A Sawatzky, "Electronic structure of Cu_2O and CuO", Physical Review. B, 38 322–330 (1988).
24. Shaveta Thakur, Neha Sharma, Anamika Varkia and Jitender Kumar, "Structural and optical properties of copper doped ZnO nanoparticles and thin films", Advances in Applied Science Research, 5 18-24 (2014).

25. M. Oztas and M. Bedir, “Thickness dependence of structural, electrical and optical properties of sprayed ZnO:Cu films”, Thin Solid Films 516 1703-1709 (2008).
26. M. B. Rahmani, S. H. Keshmiri, M. Shafiei, K. Latham, W. Wlodarski, J. du Plessis and K. Kalantar-Zadeh, “Transition n- to p-Type of Spray Pyrolysis DepositedCu Doped ZnO Thin Films for NO_2 Sensing” Sensor Letter, 7 1-8 (2009).
27. Y. Caglar, D. Oral, M. Caglar, S. Ilican, M. A. Thomas, K. Wu, Z. Sun, J. Cu, “Synthesis and characterization of (CuO)x(ZnO)1−x composite thin films with tunable optical and electrical properties”, Thin Solid Films, 520 6642–6647 (2012).
28. A. P. Moura, L. S. Cavalcante, J. C. Sczancoski, D. G. Stroppa, E.C. Paris, A. J. Ramirez, J. A. Varela, E. Longo, “Structure and growth mechanism of CuO plates obtained by microwave-hydrothermal without surfactants”, Advanced Powder Technology, 21 197-202 (2010).
29. G. Filipic, U. Cvelbar, “Copper oxide nanowires: a review of growth”, Nanotechnology, 23 194001 (2012).
30. J. B. Kim, D. Byun, S. Y. Ie, D. H. Park, W. K. Choi, C. Ji-Won, and A. Basavaraj, “Cu-doped ZnO-based p-n hetero-junction light emitting diode”, Semicond. Sci. Technol., 23 (2008).
31. N. K. Pandey, K. Tiwari, A. Tripathi, A. Roy, A. Rai, P. Awasthi, “Relative Humidity Sensing Properties of Cu_2O Doped ZnO Nanocomposite”, AIP conference Proceedings, 1147, 463, doi: 10.1063/1.3183474 (2009).
32. Nianqiang Wu, Minhua Zhao, Jian-Guo Zheng, Chuanbin Jiang, Ben Myers, Shuoxin Li, Minking Chyu and Scott X Mao, “Porous CuO–ZnO nanocomposite for sensing electrode of high-temperature CO solid-state electrochemical sensor”, Institute of Physics Publishing Nanotechnology, 16 2878–2881 (2005).
33. R. M. Allaf, L. J. Hope-Weeks, “Synthesis of ZnO-CuO nanocomposite aerogels by the sol-gel route”, J. Nanomater., 4 491817 (2014).
34. B. C. Yadav, Richa Srivastava and C. D. Dwivedi, “Synthesis and characterization of ZnO-TiO_2 Nanocomposite and its application as Humidity Sensor”, Philosophical Magazine, 88 1113-1124 (2012).
35. E.O. Omayio, P.M. Karimi, W.K. Njoroge, F.K. Mugwanga, “Current-voltage characteristics of p-CuO/n-ZnO:Sn Solar cell”, Int. J. Thin Film Sci. Technol., 2 25-28 (2013).
36. Y. Zhu, C. Haur Sow, T. Yu, Q. Zhao, P. Li, Z. Shen, D. Yu, J. Thiam-Leong Thong, “Co-synthesis of ZnO-CuO nanostructures by directly heating brass in air”, Adv. Funct. Mater, 16 2415–2422 (2006).
37. T. Soejima, K. Takada, S. Ito, “Alkaline vapor oxidation synthesis and electrocatalytic activity toward glucose oxidation of CuO/ZnO composite nanoarrays”, Appl. Surf. Sci., 277 192–200 (2013).
38. A. Zainelabdin, G. Amin, S. Zaman, O. Nur, J. Lu, L. Hultman, M. Willander, CuO/ZnO nanocorals synthesis via hydrothermal technique: growth mechanism and their application as humidity sensor, J. Mater. Chem., 22 11583–11590 (2012).
39. Q. Wei, G. Meng, X. An, Y. Hao, L. Zang, Temperature controlled growth of ZnO nanostructure: branched nanobelts and wide nanosheets, Nanotechnol, 16 2561-2566 (2005).
40. L. Chowa,O. Lupana,c, G. Chaia, H. Khallafa, L.K. Onoa, B. Roldan Cuenyaa, I.M. Tiginyanuf, V.V. Ursakif, V. Sonteac, A. Schultea, “Synthesis and characterization of Cu-doped ZnO one-dimensional structures for miniaturized sensor applications with faster response”, Sensors and Actuators, A 189 399–408 (2013).
41. S. T. Jun and G. M. Choi, “Composition of the electrical conductivity of ZnO(n) ± CuO (p) ceramic composite”, J. Amer. Ceram. Soc., 81 695-699 (1998).
42. R. E. Dietz, H. Kamimura, M. D. Sturge, and A. Yariv, “Electronic structure of copper impurities in ZnO”, Phys. Rev., 132 1559 (1963).
43. R. K. Shukla, Anchal Srivastava, Nishant Kumar, Akhilesh Pandey, Mamta Pandey, “Optical and Sensing Properties of Cu Doped ZnO Nanocrystalline Thin Films”, Journal of Nanotechnology, 2015 (2015).
44. CH. Ashok, K. Venkateswara Rao, CH. Shilpa Chakra, “Facile Synthesis and Characterization of ZnO/CuO Nanocomposite for Humidity Sensor Application”, Journal of Advanced Chemical Sciences, 2 223–226 (2016).
45. T. R. N. Kutty and N. Raghu, “Varistors based on polycrystalline ZnO:Cu”, Appl. Phys. Lett., 54 1796-1800 (1989).
46. Bi-Shiou Chiou, and Ming-Chih Chung, “Effect of Copper Additive on the Microstructure and Electrical Properties of Polycrystalline Zinc Oxide” J. Amer. Ceram. Soc., 75 3363- 3366 (1992).
47. J. V. Bellini, M. R. Morelli, and R. H. G. A. Kiminami, “Electrical properties of polycrystalline ZnO:Cu obtained from freeze-dried ZnO+copper (II) acetate powder ”, J. Mater. Sci. Mater. Electron, 13 485-489 (2002).

48. Qi Qi, Tong Zhanga,, Yi Zenga, Haibin Yang, “Humidity sensing properties of KCl-doped Cu–Zn/CuO–ZnO nanoparticles”, Sensors and Actuators B, 137 21–26, (2009).
49. V. Jeseentharani, B. Jeyaraj, J. Pragasam, A. DaySnan, and K. S. Nagaraja, “Humidity sensing properties of CuO, ZnO and NiO composites”, Sens. Transducers J., 113 48-55 (2010).
50. N. K. Pandey, Karunesh Tiwari and Akash Roy, “Moisture Sensing Application of Cu_2O Doped ZnO Nanocomposites”, IEEE Sensors Journal, 11 2142 – 2148 (2011).
51. N. K. Pandey, Tiwari Karunesh, Roy Akash, Aradhana Mishra, Anil Govindan, “Ag-Loaded WO_3 Ceramic Nanomaterials: Characterization and Moisture Sensing Studies”, Int. J Applied Ceramics Technology, 10 150–159 (2013).
52. N. K. Pandey, Tiwari Karunesh and, Akash Roy, “ZnO–TiO_2 Nanocomposite: Characterization and moisture sensing studies”, Bull. Mater. Sci., 35 347–352 (2012).
53. D. P. Singh, Jai Singh, P.R. Mishra, R. S. Tiwari, O. N. Srivastava, “Synthesis, Characterization and application of semiconducting oxide (Cu2O and ZnO) nanostructures”, Bull. Mater. Sci., 31 319-325 (2008).
54. R. L. Frost, Z. Ding, “Thermal activation of copper oxide based upon the copper hydrotalcite $Cu_xZn_{6-x}Al_2$ (OH) $16(CO_3).4H_2O$”, Thermochimica Acta, 405 207-218 (2003).
55. M. K. Deore, “Effect of CuO - Doping on Morphological and Electrical Properties of ZnO Thick Films”, International Journal of Chemical and Physical Sciences, 5 99-106 (2016).
56. T. Chang, Z. Li, G. Yun, Y. Jia, H. Yang, “Enhanced photocatalytic activity of ZnO/CuO nanocomposites synthesized by hydrothermal method”, Nano-Micro Lett., 5 163-168 (2013).
57. M.H. Habibi, B. Karimi, M. Zendehdel, M. Habibi, “Fabrication, characterization of two nano-composite CuO-ZnO working electrodes for dye-sensitized solar cell”, Spectrochim. Acta. A. Mol. Biomol. Spectrosc., 116 374-380 (2013).
58. B. Li, Y. Wang, “Facile synthesis and photocatalytic activity of ZnO-CuO nanocomposite”, Superlattice Microst., 47 615-623 (2010).
59. G. Chaitanya Lakshmi, S. Ananda, R. Somashekar, C. Ranganathaiah, Synthesis of ZnO/MgO nanocomposites by electrochemical method for photocatalytic degradation kinetics of Eosin yellow dye, Int. J. Nano Sci. Nanotechnol., 3 47-63 (2012).
60. R.N. Gedye, F.E. Smith, K.C. Westaway, The rapid synthesis of organic compounds in microwave ovens, Can. J. Chem., 66 17-26 (1988).
61. V. K. Pecharsky, P. Y. Zavalij, “Fundamentals of powder diffraction and structural characterization of materials”, Springer, New York, 2003.
62. C. Suranarayana, M. G. Norton, X-ray Diffraction: A Practical Approach, New York, 1998.
63. Chih-Hung Hsu, Lung-Chien Chen and Xiuyu Zhang, “Effect of the Cu Source on Optical Properties of Cu-ZnO Films Deposited by Ultrasonic Spraying”, Materials, 7 1261-1270 (2014).
64. J. Ghijsen, L.H Tjeng, J. van Elp, H. Eskes, J. Westerink, and G.A Sawatzky, “Electronic structure of Cu_2O and CuO”, Physical Review. B, 38 322–330 (1988).
65. Shaveta Thakur, Neha Sharma, Anamika Varkia and Jitender Kumar, “Structural and optical properties of copper doped ZnO nanoparticles and thin films”, Advances in Applied Science Research, 5 18-24 (2014).
66. M. Oztas and M. Bedir, “Thickness dependence of structural, electrical and optical properties of sprayed ZnO:Cu films”, Thin Solid Films 516 1703-1709 (2008).
67. M. B. Rahmani, S. H. Keshmiri, M. Shafiei, K. Latham, W. Wlodarski, J. du Plessis and K. Kalantar-Zadeh, “Transition n- to p-Type of Spray Pyrolysis Deposited Cu Doped ZnO Thin Films for NO_2 Sensing” Sensor Letter, 7 1-8 (2009).
68. Y. Caglar, D. Oral, M. Caglar, S. Ilican, M. A. Thomas, K. Wu, Z. Sun, J. Cu, “Synthesis and characterization of (CuO)x(ZnO)1−x composite thin films with tunable optical and electrical properties”, Thin Solid Films, 520 6642–6647 (2012).
69. A. P. Moura, L. S. Cavalcante, J. C. Sczancoski, D. G. Stroppa, E.C. Paris, A. J. Ramirez, J. A. Varela, E. Longo, “Structure and growth mechanism of CuO plates obtained by microwave-hydrothermal without surfactants”, Advanced Powder Technology, 21 197-202 (2010).
70. G. Filipic, U. Cvelbar, “Copper oxide nanowires: a review of growth”, Nanotechnology, 23 194001 (2012).
71. J. B. Kim, D. Byun, S. Y. Ie, D. H. Park, W. K. Choi, C. Ji-Won, and A. Basavaraj, “Cu-doped ZnO-based p-n hetero-junction light emitting diode”, Semicond. Sci. Technol., 23 (2008).

72. N. K. Pandey, K. Tiwari, A. Tripathi, A. Roy, A. Rai, P. Awasthi, "Relative Humidity Sensing Properties of Cu_2O Doped ZnO Nanocomposite", AIP conference Proceedings, 1147, 463, doi: 10.1063/1.3183474 (2009).
73. Nianqiang Wu, Minhua Zhao, Jian-Guo Zheng, Chuanbin Jiang, Ben Myers, Shuoxin Li, Minking Chyu and Scott X Mao, "Porous CuO–ZnO nanocomposite for sensing electrode of high-temperature CO solid-state electrochemical sensor", Institute of Physics Publishing Nanotechnology, 16 2878–2881 (2005).
74. R. M. Allaf, L. J. Hope-Weeks, "Synthesis of ZnO-CuO nanocomposite aerogels by the sol-gel route", J. Nanomater., 4 491817 (2014).
75. B. C. Yadav, Richa Srivastava and C. D. Dwivedi, "Synthesis and characterization of ZnO-TiO_2 Nanocomposite and its application as Humidity Sensor", Philosophical Magazine, 88 1113-1124 (2012).
76. E.O. Omayio, P.M. Karimi, W.K. Njoroge, F.K. Mugwanga, "Current-voltage characteristics of p-CuO/n-ZnO:Sn Solar cell", Int. J. Thin Film Sci. Technol., 2 25-28 (2013).
77. Y. Zhu, C. Haur Sow, T. Yu, Q. Zhao, P. Li, Z. Shen, D. Yu, J. Thiam-Leong Thong, "Co-synthesis of ZnO-CuO nanostructures by directly heating brass in air", Adv. Funct. Mater, 16 2415–2422 (2006).
78. T. Soejima, K. Takada, S. Ito, "Alkaline vapor oxidation synthesis and electrocatalytic activity toward glucose oxidation of CuO/ZnO composite nanoarrays", Appl. Surf. Sci., 277 192–200 (2013).
79. A. Zainelabdin, G. Amin, S. Zaman, O. Nur, J. Lu, L. Hultman, M. Willander, CuO/ZnO nanocorals synthesis via hydrothermal technique: growth mechanism and their application as humidity sensor, J. Mater. Chem., 22 11583–11590 (2012).
80. Q. Wei, G. Meng, X. An, Y. Hao, L. Zang, Temperature controlled growth of ZnO nanostructure: branched nanobelts and wide nanosheets, Nanotechnol, 16 2561-2566 (2005).
81. L. Chowa,O. Lupana,c, G. Chaia, H. Khallafa, L.K. Onoa, B. Roldan Cuenyaa, I.M. Tiginyanuf, V.V. Ursakif, V. Sonteac, A. Schultea, "Synthesis and characterization of Cu-doped ZnO one-dimensional structures for miniaturized sensor applications with faster response", Sensors and Actuators, A 189 399–408 (2013).
82. S. T. Jun and G. M. Choi, "Composition of the electrical conductivity of ZnO(n) ± CuO (p) ceramic composite", J. Amer. Ceram. Soc., 81 695-699 (1998).
83. R. E. Dietz, H. Kamimura, M. D. Sturge, and A. Yariv, "Electronic structure of copper impurities in ZnO", Phys. Rev., 132 1559 (1963).
84. CH. Ashok, K. Venkateswara Rao, CH. Shilpa Chakra, "Facile Synthesis and Characterization of ZnO/CuO Nanocomposite for Humidity Sensor Application", Journal of Advanced Chemical Sciences, 2 223–226 (2016).
85. T. R. N. Kutty and N. Raghu, "Varistors based on polycrystalline ZnO:Cu", Appl. Phys. Lett., 54 1796-1800 (1989).
86. Qi Qi, Tong Zhanga,, Yi Zenga, Haibin Yang, "Humidity sensing properties of KCl-doped Cu–Zn/CuO–ZnO nanoparticles", Sensors and Actuators B, 137 21–26, (2009).
87. V. Jeseentharani, B. Jeyaraj, J. Pragasam, A. DaySnan, and K. S. Nagaraja, "Humidity sensing properties of CuO, ZnO and NiO composites", Sens. Transducers J., 113 48-55 (2010).
88. N. K. Pandey, Karunesh Tiwari and Akash Roy, "Moisture Sensing Application of Cu_2O Doped ZnO Nanocomposites", IEEE Sensors Journal, 11 2142 – 2148 (2011).
89. N. K. Pandey, Tiwari Karunesh, Roy Akash, Aradhana Mishra, Anil Govindan, "Ag-Loaded WO_3 Ceramic Nanomaterials: Characterization and Moisture Sensing Studies", Int. J Applied Ceramics Technology, 10 150–159 (2013).
90. N. K. Pandey, Tiwari Karunesh and, Akash Roy, "ZnO–TiO_2 Nanocomposite: Characterization and moisture sensing studies", Bull. Mater. Sci., 35 347–352 (2012).

CHAPTER II

Moisture Sensing Studies of Nanostructured Cu-doped ZnO Thin Films

2.1. Sample Preparation and Experimental Process

Cu-doped ZnO thin films were developed in the experimental process. Zinc acetate ($Zn(CH_3COO)_2.2H_2O$) was used as starting material, methanol as organic solvent and monoethanolamine (MEA) as surfactant. All the sols were prepared in a volume of 50 cc and concentration of 0.5 M. Zinc acetate dihydrate was dissolved in a mixture of methanol and monoethanolamine at room temperature. For the doping of Cu, copper sulphate was used and the doping percentages were 1, 3, 5, 7 and 8 atomic%. Then each of the mixture prepared was vigorously stirred by a magnetic bar for 2 hours. The solution then became homogeneous and allowed to age for 24 hours. Then, the aged solution was used for the preparation of thin films using a spin coating device. The prepared solution was spin coated at a speed of 3000 rpm for 30 seconds on glass substrate for the development of thin films. Thin films were annealed in air from 300°C to 600°C for 3 hours in an electric muffle furnace. After annealing, samples were analyzed for activation energy and humidity sensing studies. The prepared thin film samples were labeled as CZ-1 (1 at% Cu doping in ZnO), CZ-3 (3 at% Cu doping in ZnO), CZ-5 (5 at% Cu doping in ZnO), CZ-7 (7 at% Cu doping in ZnO) and CZ-8 (8 at% Cu doping in ZnO). The undoped ZnO thin films were prepared using a spin coating device and the sample was labeled as CZ-0. The thickness of the CZ-7 thin film annealed at 600°C was found to be 780 nm (using Dektak Surface Profilometer). The thickness of the CZ-0 thin film annealed at 600°C was found to be 960 nm.

2.2. Scanning Electron Microscope (Sem) Study

Figure 2.1 shows SEM of CZ-0 and CZ-1 SEM micrographs of the thin films CZ-0 (undoped ZnO) and CZ-7 annealed at temperature 600°C, respectively. From the SEM it is observed that grains of nanomaterial formed are scattered all over the substrate and a network of pores is formed. These pores are responsible for the formation of sites for humidity adsorption. As annealing temperature increases it is found that

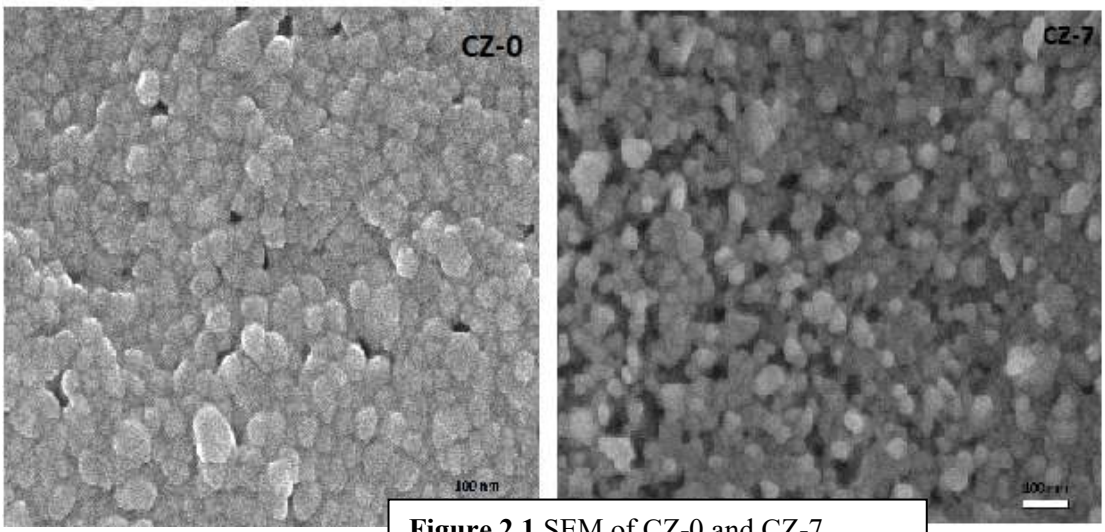

Figure 2.1 SEM of CZ-0 and CZ-7

porosity of the material increases. The porous structure is dependent on the composition. The pore structures should be regarded as voids that form a kind of capillary tubes. This structure favors the enhanced rate of adsorption and desorption of water molecules. The average grain size calculated from SEM micrograph for sensing elements CZ-0, CZ-1, CZ-3, CZ-5, CZ-7 and CZ-8 are shown in Table 2.1. The average grain size for the sensing elements CZ-7 and CZ-0 calculated from SEM micrographs are 36 nm and 42 nm, respectively.

2.3. X-Ray Diffraction Analysis

Figure 2.2 shows X-ray pattern for the sensing elements CZ-0 and CZ-7 annealed at 600°C. The crystallite size for the sensing elements CZ-0 and CZ-7 annealed at 600°C are in the 24–38 nm and 25–41 nm range, respectively.

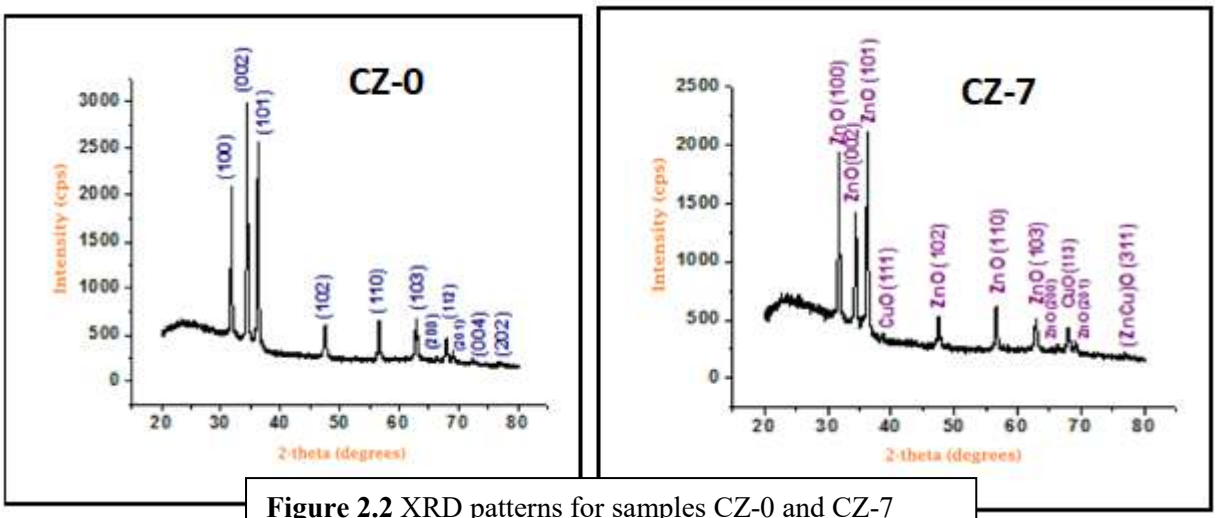

Figure 2.2 XRD patterns for samples CZ-0 and CZ-7

2.4. Experimental

A special humidity control chamber was designed for performing humidity sensing studies. For the calibration purpose, standard hygrometer, and a thermometer was used inside this chamber. Potassium sulphate was used as a humidifier and potassium hydroxide was used a dehumidifier in the experiment. The change in resistance was recorded with change in RH (relative humidity). Standard hygrometer was used for measuring RH. Resistance variation of the thin films was recorded using a resistance meter (±0.001MΩ, model: CHY 21). For measuring the resistance of the thin films we have prepared silver electrodes. For making the electrical contacts on the surface of the thin films, silver electrodes were developed at the ends of the thin films. After performing the study of humidity sensing properties, sensing elements were kept in laboratory environment and their humidity sensing characteristics were regularly monitored. To see the effect of ageing, the sensing properties of these sensing elements were examined again in the humidity control chamber after a span of six months.

2.5. Sensing Mechanism

As the humidity increases, excess protons (H^+) start diffusing through the hydrogen bond network of molecules. In other words, protons (H^+) start tunnelling from one water molecule to the next through hydrogen bonding. During first stage of adsorption water molecules come in contact with the material and an adsortion complex is formed. This phenomenon is known as chemisorption. During further adsorption, the adsorption complex forms bonds with the water molecules through hydroxyl groups and hence water molecules get adsorbed on the surface through hydrogen bonding. This is physical adsorption. So, during the first physisorption the layer formed is immobile due to the absence of the hydrogen bonds formed between the water molecules in this layer. Therefore, no proton (H^+) could be conducted in this stage. When the relative humidity (RH) increases, mobile layers of water molecules are formed with the presence of hydrogen bonds between water molecules and this is responsible for the conduction of protons in this stage. Sometimes due to the breaking of bonds and formation of new bonds the path of proton conduction changes. Due to this there is sudden change in the surface energy of the thin fims. Due to sudden change in the surface energy, hysteresis phenomenon may arise. Either ionic or electronic type mechanism is responsible for the conduction mechanism in the sensors based on the ceramic materials. Electrons are donated by the water molecules in the electronic type mechanism. These water molecules get chemisorbed and hence in this way the electronic conductivity gets increased or decreased. This conductivity actually depends on the fact whether the material is p-type or n-type semiconductor. If the mechanism is ionic type then the impedance of the sensor decreases with increase in the value of RH due to the increase in the proton (H^+) conductivity in the physisorbed layers. As soon as the nanomaterials developed from the undoped and doped ZnO come in contact with humid air, the chemisorption process starts and the water molecules chemisorb on the available sites of the material surface. Firstly, the chemisorbed layer is formed due to the chemisorption process and thereafter the physisorbed layers are formed. Moreover, the electrons may also get accumulated at the surface of undoped and doped ZnO and consequently, the resistance of the sensing element decreases with increase in RH (relative humidity). Cu-doped ZnO thin films enhance the adsorption and desorption rates of the water molecules and hence helps in increasing the sensitivity of the material.

2.6. Results and Discussion

For sensing elements CZ-1, CZ-3, CZ-5, CZ-7 and CZ-8 annealed at 600 ºC, a graph has been plotted between resistance and %RH for the humidification process and is shown in Figure 2.3. A continuous decrease in the value of resistance is seen with increase in the %RH for all these sensing elements in the 15%–95% RH range. There is continuous decrease in the value of resistance with increase in the %RH for all these sensing elements.

All the sensing elements of Cu-doped ZnO thin

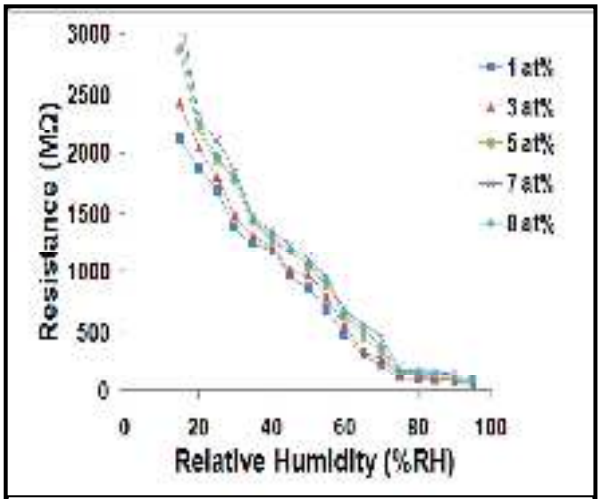

Figure 2.3 Resistance Vs Humdity Graph

films are showing sharp decline in the values of resistance up to relative humidity 75% RH while that in the case of undoped ZnO thin films sharp decline can be seen in the values of resistance up to relative humidity 60% RH. If the porosity of the material increases then due to this surface to volume ratio of the materials also increases and hence the process of diffusion of water molecules into or out of the pores also increases; and in this way good sensitivity is achieved. When the RH becomes high (>75% RH) then the water molecules in the capillary like pores condenses due to which a liquid like layer is formed. If there is variation of grain boundary barrier height then also the resistance may decrease. In this case, adsorption of water molecules at metal oxide surface penetrated inside the sample can decrease the height of potential barriers at the surface of grains and at the surface of necks between metal oxide grains. Therefore, size of depletion regions in the vicinity of necks in the direction of electric field is lowered and conductance of ceramics is increased. When the water molecules get penetrated inside the pores then there may be decrease in barrier height of grain boundary potential in an exponential manner and even slight decrease of grain boundary barrier height due to RH can cause considerable decrease of resistance (or increase of conductance).

2.7. Regression Analysis

A regression analysis of the humidification graphs of undoped and Cu-doped ZnO was carried out. A polynomial of sixth degree (given below) fitted to the curve of resistance versus %RH graph of the sensing element CZ-7 annealed at 600°C.

$y = 2\times10^{-08}\,x^6 - 2\times10^{-05}x^5 + 0.003x^4 - 0.417x^3 + 22.56x^2 - 626.3x + 8744$ (2.1)

Here, x= %RH and y= resistance in MΩ

Moreover, it is also found that a polynomial of third degree (given below) fitted to the curve of sensitivity versus temperature graph of the sensing element CZ-7.

$y = -4\times10^{-07}x^3 + 0.000x^2 - 0.195x + 47.08$ (2.2)

Here, x= temperature and y= sensitivity in MΩ/%RH

Also, for the sample CZ-0 a polynomial of third degree (given below) fitted to the curve of sensitivity versus temperature graph.

$y = 5\times10^{-08}x^3 - 9\times10^{-05}x^2 + 0.075x - 1.94$ (2.3)

Here, x= temperature and y= sensitivity in MΩ/%RH

2.8. Sensitivity

Sensitivity of Cu-doped ZnO thin films for all sensing elements for annealing temperatures 300°C–600°C are shown in Table 2.2. Sensitivity of undoped ZnO thin films for annealing temperatures 300°C–600°C are shown in Table 2.3. The sensing element developed from undoped ZnO thin film and annealed at 600°C showed good results with an average sensitivity of 20.63 MΩ/%RH. The sensing element CZ-7 thin film annealed at 600°C showed the best results with an average sensitivity of 39.14 MΩ/%RH. So, an increase in the value of sensitivity for Cu-doped ZnO thin films sensing element was noticed over that of undoped ZnO. For sensing

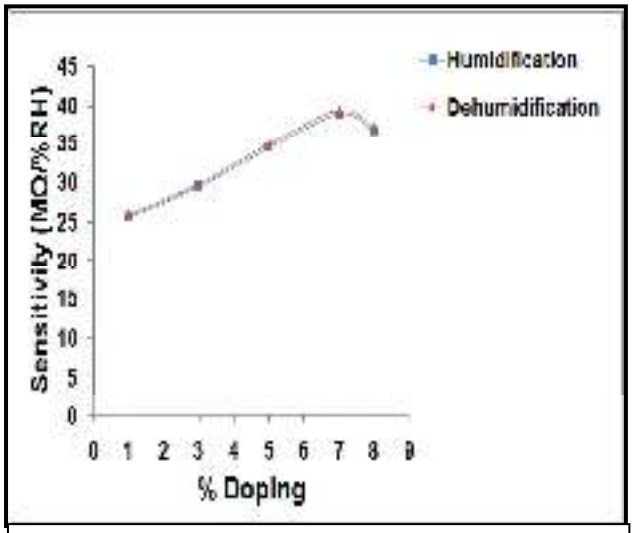

Figure 2.4 Sensitivity Vs Doping % Graph

element of Cu-doped ZnO thin films annealed at 600°C, the sensitivity is found to be repeatable within ±2.00% in dehumidification cycle of relative humidity and within ±1.5% over humidification cycle of relative humidity after six months. It has been observed that adsorption sites (or pores) increases with increase in the annealing temperature. Higher porosity increases surface to volume ratio of the materials and therefore, helps in getting good sensitivity. This increases the sensitivity of the sensing elements. With the increase in the Cu-doping percentage the grain size increases and these grains are randomly distributed all over the surface due to which the probability of the formation of pores increases which leads to the increase in the sensitivity. Figure 2.4 shows variation of sensitivity with %doping for the Cu-doped ZnO sensing elements annealed at 600°C for humidification processes. For the sensing elements CZ-1, CZ-3, CZ-5 and CZ-7 annealed at 600°C sensitivity increases with the increase in the doping percentage.

Hysteresis was found to decrease with increase in the annealing temperature for sensing elements of CZ-7 thin films; values of hysteresis being 2.64%, 2.16%, 1.41% and 1.02% for annealing temperatures 300°C, 400°C, 500°C and 600°C, respectively. For sensing element CZ-0, hysteresis values are 3.64%, 3.12%, 2.64% and 1.38% for annealing temperatures 300°C, 400°C, 500°C and 600°C, respectively. So, a decrease in the value of hysteresis was observed in the case of Cu-doped ZnO sensing element annealed at 600°C over that of undoped ZnO. As a matter of fact, the energy required for the removal of the physisorbed layer is very less in comparison to the energy required for the removal of chemisorbed layer. With the increase in the annealing temperature the porosity of the thin films increases due to which the probability of physisorption process increases as compared to the chemisorption process. That is why hysteresis decreases with the increased annealing temperature. The nanomaterials formed provide enhanced adsorption capability, good sensitivity values, and low hysteresis.

Variation of resistance of all the sensing elements with change in %RH after six months was analyzed. For all the sensing elements annealed at 600°C, values were generally repeatable within ±2.00% in the 15–95% RH range after six months.

As the annealing temperature increases the value of response/recovery time decreases i.e., the response and recovery are getting faster with increase in annealing temperature. Response/recovery time for the sensing element CZ-0 (undoped ZnO) for the annealing temperatures 300°C, 400°C, 500°C and 600°C are 112/180, 95/147, 79/116 and 67/94 seconds, respectively. Response/recovery time for the sensing element CZ-7 for the annealing temperatures 300°C, 400°C, 500°C and 600°C are 73/92, 59/78, 45/62 and 32/47 seconds, respectively. Thus, Cu-doped ZnO thin films gave better response and recovery time compared to the sensing element of undoped ZnO. Desorption of the water molecules is a slow process; therefore, the recovery time is always greater than the response time.

Activation energy (ΔE) measures the thermal or other form of energy required to raise electrons from the donor levels to the conduction band or to accept electrons by the acceptor levels E_a from the valence band respectively for n- and p-type semiconductor materials. Activation energy corresponds to the energy difference (E_c-E_d) and (E_a-E_v) respectively for n- and p-type semiconductor materials. Equation (1) gives the activation energy value.

$$R = R_o\, e^{-\Delta E/2kT} \quad (2.4)$$

Therefore, $\ln (R) = \ln(R_o) - \Delta E/2kT$ (2.5)

Here, R=resistance, R_o=constant, ΔE=activation energy of electronic transport, k=Boltzmann's constant and T=absolute temperature.

From the slope of the plot ln(R) versus 10000/T graph [using Eq. (2.5)], value of activation energy for electronic transport may be calculated. range Sample of Cu-doped ZnO nanomaterial showed low value of activation energy indicating that this sensing element had low operating temperature and could be used at room temperature as well.

Table 2.1 Grain Size by SEM (nm)

CZ-1	CZ-3	CZ-5	CZ-7	CZ-8	CZ-0
18	24	29	36	45	42

TABLE 2.2 Sensitivity of Samples of Undoped ZnO

Annealing Temperature	Sensitivity (MΩ/%RH) (Undoped ZnO)		
	a	b	c
300 ºC	13.63	13.79	13.26
400 ºC	16.53	16.67	16.18
500 ºC	18.74	18.88	18.39
600 ºC	20.58	20.68	20.12
[a]Increasing cycle of relative humidity; [b]Decreasing cycle of relative humidity; [c]Increasing cycle after six months			

TABLE 2.3 Sensitivity of Doped samples (MΩ/%RH)

Annealing Temp.	Sample (CZ-1)			Sample (CZ-3)			Sample (CZ-5)			Sample (CZ-7)			Sample (CZ-8)		
	a	b	c	a	b	c	a	b	c	a	b	c	a	b	c
300 ºC	15.79	16.07	15.38	19.42	19.74	19.17	24.68	24.96	24.35	25.82	26.19	25.48	22.56	22.91	22.31
400 ºC	18.48	18.74	18.05	23.68	23.94	23.34	27.73	28.06	27.42	29.48	29.80	29.16	27.41	27.76	27.13
500 ºC	22.37	22.68	22.10	26.64	26.95	26.31	30.86	31.16	30.54	34.61	34.94	34.36	32.62	32.97	32.39
600 ºC	25.63	25.98	25.34	29.54	29.87	29.26	34.58	35.02	34.27	38.94	39.34	38.61	36.78	37.18	36.27

[a]Increasing cycle of relative humidity; [b]Decreasing cycle of relative humidity; [c]Increasing cycle after six months

CHAPTER III

Analysis on Activation Energy and Humidity Sensing Application of Nanostructured SnO_2-doped ZnO Material

This chapter reports analysis on activation energy and humidity sensing studies of SnO_2-doped ZnO nanomaterial. Pellets of SnO_2-doped ZnO nanomaterial were prepared by applying pressure of 260 M Pa. The prepared pellets were annealed at different temperatures. Activation energy analysis was done on the Arrhenius plot. Low values of activation energy suggested low operating temperature for the samples and hence could be used at room temperature. The humidity sensing studies of these samples were also analyzed. Sensing element annealed at 700ºC showed the best results with sensitivity of 32.16 MΩ/%RH. The properties like lower hysteresis, less effect of ageing and high reproducibility were exhibited by the sample annealed at 700°C. The sensitivity increased with increase in annealing temperature. Other parameters like response time, recovery time, hysteresis and ageing effects were also studied. The crystallite size from XRD was in the 27-155 nm range. The average grain size as measured from SEM micrograph was 198 nm. From the SEM micrograph it became clear that agglomeration of smaller crystallites is occurring to form larger grains.

3.1 Activation Energy

From the slope of the plot ln(R) versus 1/T graph, values of activation energy for electronic transport may be calculated. Figure 1 shows Arrhenius Graph for Activation Energy for 1% SnO_2-doped ZnO sample (SZ). The activation energy values for sample SZ from the Arrhenius plot is found to be 0.178 eV for temperature range 60°C to 140°C and 0.10025 eV for 140°C to 200°C, indicating that there are two different inter-band transitions for electrons. Sample of SnO_2 doped ZnO nanomaterial showed lower values of activation energy in the two regions indicating that this sensing element had lower operating temperatures and could be used at room temperature.

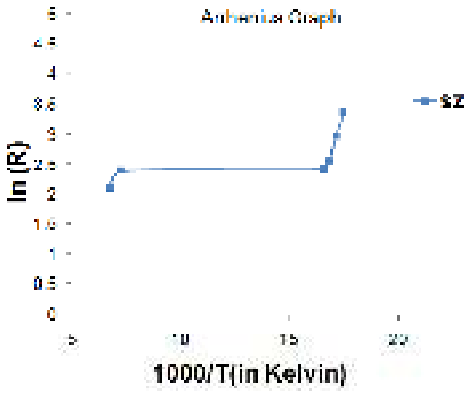

Figure 3.1 Arrhenius Graph

3.2 Scanning Electron Microscope Study

From the SEM it is observed that grains of ZnO are scattered all over the substrate and a network of pores and flakes is formed. These pores are responsible for the formation of sites for humidity adsorption. SEM micrograph for the sample SZ annealed at 700°C is shown in Figure 3.2. The SEM micrograph of this sensing element shows great clustering and agglomeration of large number of crystallites. The average grain size calculated from SEM micrograph for this sensing element is 198 nm. The sensing element in the case of undoped

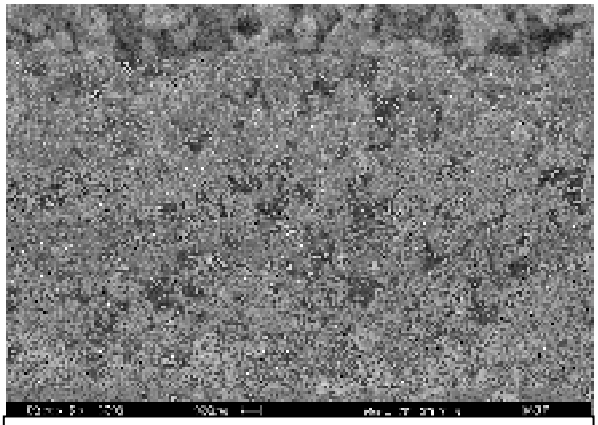

Figure 3.2 SEM for SZ Sample

ZnO manifests low porosity in comparison to the sensing element of SnO_2-doped ZnO nanomaterial. Due to this SnO_2-doped ZnO nanomaterial has enhanced adsorption and desorption rates which is responsible for better sensitivity, low hysteresis and better response and recovery time compared to undoped ZnO.

3.3 X-Ray Diffraction Analysis

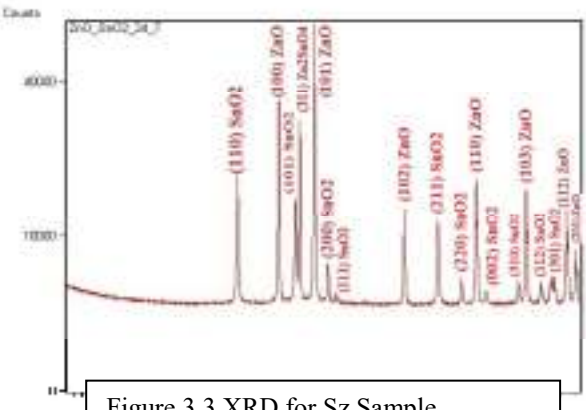

Figure 3.3 XRD for Sz Sample

Figure shows X-ray pattern for the sensing element SZ annealed at 700°C. Using Scherrer's formula the sample's average crystallite size was calculated. The crystallite size for SZ annealed at 700°C calculated from Scherrer's formula is in the 27-155 nm range.

3.4 Results and Discussion

In Figure 3.4 a graph is plotted between resistance and % RH for the sensing elements for the humidification process. From the graph it is clear that for all the sensing elements the resistance decreases as the % RH increases. Sensing element SZ annealed at 700°C shows low hysteresis value within acceptable limits. The sensitivity value increases with the increase in the annealing temperature. The best sensitivity value is 32.16 MΩ/%RH for the sample SZ annealed at 700°C. Due to the excellent electrical properties and enhanced adsorption capability of the nanomaterials SZ it can prove to be an excellent humidity sensor.

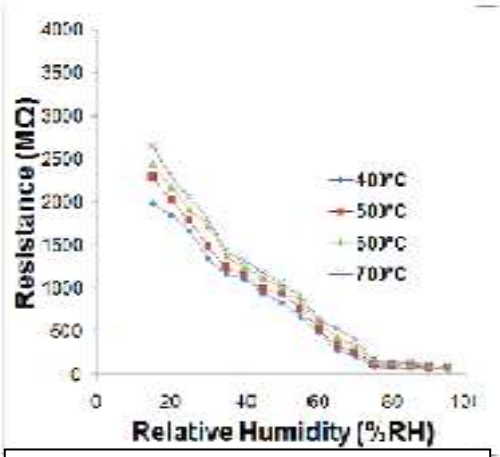

Figure 3.4 Resistance Vs % RH

A polynomial of sixth degree (given below) fitted to the curve of resistance versus %RH (Relative Humidity) graph of the sensing element SZ annealed at 700°C.

$$y = -3\times10^{-07}\,x^6 + 0.000x^5 - 0.013x^4 + 0.829x^3 - 26.13x^2 + 331.1x + 1347. \quad (4)$$

Here, x= %RH (Relative Humidity) and y= Resistance in MΩ

Moreover, it is also found that a polynomial of third degree (given below) fitted to the curve of sensitivity versus temperature graph of the sensing element SZ.

$$y = 4\times10^{-07}\,x^3 - 0.000x^2 + 0.436x - 59.61 \quad (5)$$

Here, x= Temperature and y= Sensitivity in MΩ/%RH

Figure 3.5 shows sensitivity versus temperature graphs for the sensing elements SZ annealed at different temperatures. From figure it is clear that the sensitivity increases with the increasing annealing temperature.The best sensitivity value observed is 32.16 MΩ/%RH for the sample SZ annealed at 700°C. The sensing element developed from undoped ZnO and annealed at 700°C showed good results with an average sensivity of 12.35 MΩ/%RH. So, an increase by 160% in the value of sensitivity for SnO_2-doped ZnO sensing element was noticed over that of ZnO. For sensing

element SZ annealed at 700°C, the sensitivity is found to be repeatable within ±2.00% after six months. SnO_2 doping enhances the electrical response of ZnO. Higher porosity increases surface to volume ratio of the materials and therefore, helps in getting good sensitivity. An analysis of the crystallite size and grain size would suggest that smaller crystallites are getting agglomerated to form larger grains. In this process, more of the surface areas of the sensing elements are exposed leading to more adsorption of water molecules. This increases the sensitivity of the sensing elements.

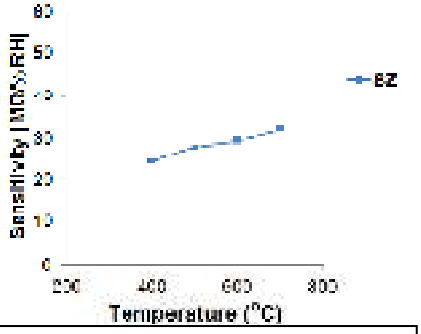

Figure 3.5 Sensitivity Vs Annealing Temperture

All sensing elements manifest acceptable hysteresis values. Hysteresis was found to decrease with increase in the annealing temperature for sensing element SZ; values of hysteresis being 3.62%, 2.70%, 2.16% and 1.17% for annealing temperatures 400°C, 500°C, 600°C and 700°C, respectively. The sensing element developed from undoped ZnO and annealed at 700°C showed hysteresis of 1.89%. So, a decrease in the value of hysteresis by 38% was observed in the case of SnO_2-doped ZnO sensing element annealed at 700°C over that of ZnO. Sensing element SZ annealed at 700°C shows lowest hysteresis value within acceptable limits. The nanocomposites formed provide enhanced adsorption capability, good sensitivity values and low hysteresis.

Variation of resistance of all the sensing elements with change in % RH after six months was analyzed. For all the sensing elements annealed at 700°C, values were generally repeatable within ±1.70% in the 10%–90% RH range after six months. All the sensing elements showed significantly less ageing effect in their performance for all the annealing temperatures considered. The sensing elements of both undoped ZnO and SnO_2-doped ZnO showed significantly less ageing effects in their performance for all the annealing temperatures considered.

The response and recovery are getting faster with increase in annealing temperature. Response and recovery time for the sensing element SZ for the annealing temperature 700°C were 74 and 212 seconds, respectively. The response and recovery time for the sensing element of undoped ZnO annealed at 700°C were 91 and 315 seconds, respectively. Thus, SnO_2-doped ZnO nanomaterial gave better response and recovery time compared to the sensing element of undoped ZnO. Figure 3.6 shows graphs for response time and recovery time.

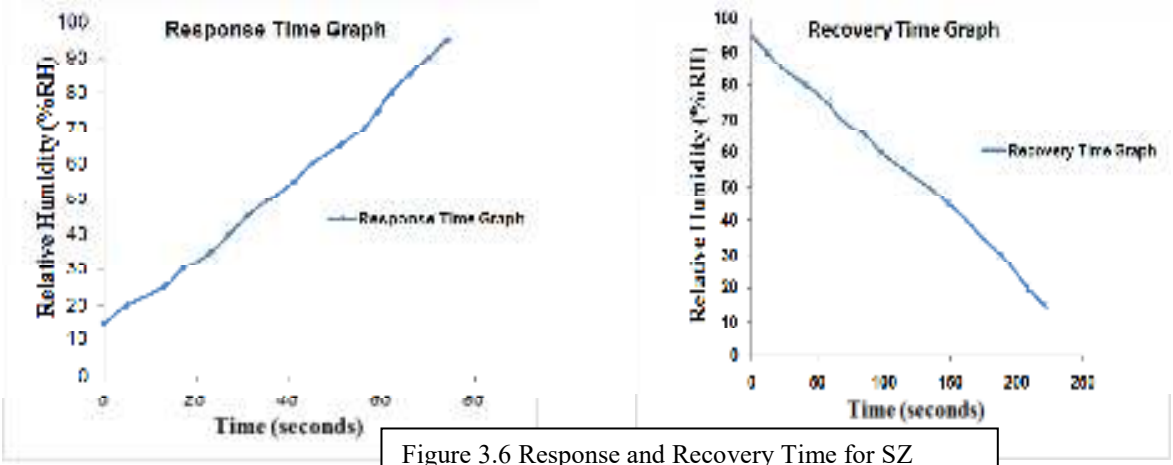

Figure 3.6 Response and Recovery Time for SZ

CHAPTER IV

MnO_2-ZnO Hexagonal Nanomaterials: Characterization and High Performance Humidity Sensing Application

In present investigation, undoped and MnO_2 doped nanostructured zinc oxide was synthesized by solid state reaction route. The prepared material was characterized by X-ray diffraction, scanning electron microscope and UV-Vis absorption spectroscopy. X-ray diffraction study confirmed the presence of zinc oxide and its minimum average crystallite size was 47.5 nm. The doping of MnO_2 enhanced the crystallization and decreased the crystallite size. The minimum average crystallite size was 31.7 nm for 1.0 weight% MnO_2 doped zinc oxide. Surface morphology of the sensing material showed that the hexagonal shaped particles were uniformly distributed in zinc oxide that left large number of pores. These pores acted as humidity adsorption sites. With increase in the concentration of MnO_2, the pores also increased. The optical band gap of the undoped zinc oxide was 4.05 eV. The value of band gap decreased with increase in the MnO_2 doping concentration. The average sensitivity of undoped zinc oxide was 3400 KΩ/%RH. The sensitivity increased with increase in the doping concentration.

4.1 Introduction

The present work shows very high sensitivity compared to many reported works; more than six times the sensitivity of Ag-WO_3 nanomaterial and nearly four times Cu_2O-ZnO sensor, more than 1.5 times WO_3-SnO_2 sensor. The hysteresis and aging in all cases were within ±2%.

4.2 Synthesis of ZnO-MnO_2 Composite Pellets

The starting material was ZnO (Loba Chemie 98.0%). For binding the material 5% by weight of ethyl cellulose (LobaChemie) was used. The mixture was grinded for 3 hoursto homogeneity, and smaller crystalline size. The fine and grained powder of sample was pelletized with the help of hydraulic press machine (M.B. Instruments, Delhi, India) under an uniaxial pressure of 4 M Pa at room temperature. The pellets, then, were annealed for good nucleation and growth of the grains which were required for the sensing. This made surface to volume ratio higher. Sensing elements with 0%, 0.2%, 0.4%, 0.6%, 0.8% and 1.0% of MnO_2 in ZnO are labelled as Z_1, Z_2, Z_3, Z_4, Z_5 and Z_6, respectively.

4.3 UV-Vis Spectroscopy

UV–Vis absorption spectrophotometer (Model− V670, Jasco) in UV and visible ranges from 200-800 nm was used for optical measurements. The typical UV-visible spectra of MnO_2 doped zinc oxide are shown in the Figure 1.1. The spectrum of each composition shows a sharp intense absorption band at energies close to the optical band gap that manifests itself as an absorption edge (as shown in Figure 1a). The optical band gap is calculated by extrapolation of linear plot (Tauc plot) between absorption coefficient (α) and photon energy as described in given equation:

$$\alpha(h\nu) = (h\nu - E_g)^{1/2} \quad (1)$$

here, E is the photon energy and E_g is the optical band gap energy of the material. This equation shows a linear dependence of $\alpha^2(h\upsilon)$ on photon energy (E). Figure 1(b) shows the Tauc plots of α^2 ($h\upsilon$) versus photon energy ($h\upsilon$). The optical band gap of undoped zinc oxide was found 4.05 eV. The value of optical band gap decreased with increase in MnO_2 concentration. The decrease in the value

of band gap in the present study shows the red shift with increase of MnO_2concentration. Value of optical band gap are 4.05, 4.05, 4.02, 3.95, 3.90 and 3.85 for 0.0%, 0.2%, 0.4%, 0.6%, 0.8% and 1.0% doping of MnO_2 in ZnO, respectively.

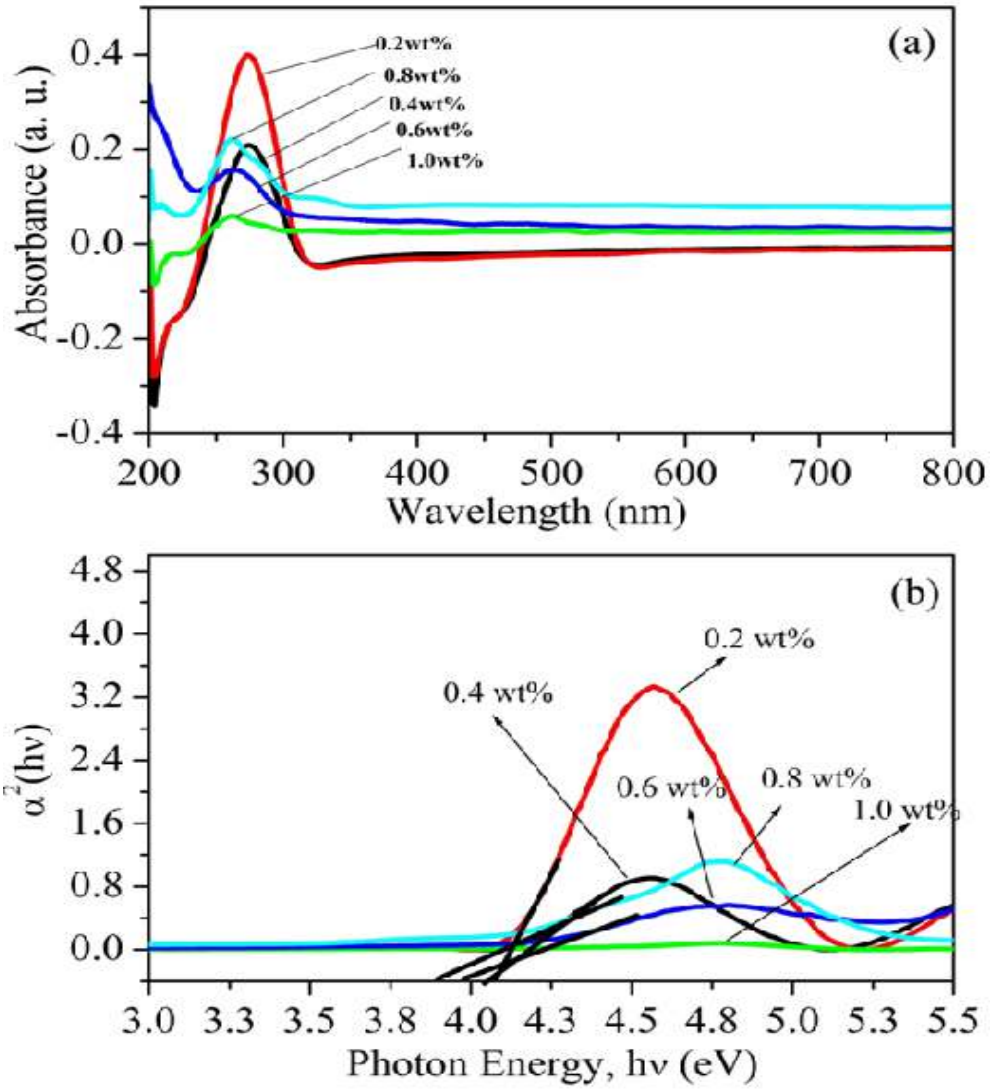

Figure 4.1 UV-Visible spectroscopy of ZnO-MnO_2 in the wave number 200-800 annealed at 600˚C (a) for sensing elements Z_1, Z_2, Z_3, Z_4, Z_5 and Z_6. (b) Tauc plots of α^2 (hυ) versus photon energy (hυ) for sensing elements Z_1, Z_2, Z_3, Z_4, Z_5 and Z_6.

4.4 Scanning Electron Microscopy

Annealing process reduces the residual stress on the surface of the materials. The grains become ordered in a specific manner leaving some more spaces among them. Due to the annealing process, the size of pores increases. The re-crystallization process during the annealing has two stages, in the beginning; the re-crystallization is dominated by random orientation of the grains followed by a

second process in which once again the crystallites tend to orient in a particular direction. Due to their particular orientation/alignment, the surface morphology changes. The typical microstructure of undoped and 0.2, 0.4, 0.6, 0.8 and 1.0 weight% MnO_2 doped zinc oxide and annealed at temperatures 600˚C are shown in Figures 4.2 (a-f). Figure 4(a) reveals that nanoparticles of ZnO agglomerate with one another leaving some spaces as pores. These pores serve as humidity adsorption sites and humidity sensitivity of the sensor depends on the size of these pores. Most of the particles are hexagonal in shape leaving more space as pores, giving effective surface area due to nano-sized surface morphology. The microstructure of 0.2 weight% MnO_2 doped zinc oxide shows almost similar pattern microstructure as that of pure ZnO, only a little bit difference of degree of crystallization and pores size [as shown in Figure 4.2(b)]. As the doping % of MnO_2 was increased from 0.2 weight% to 0.4 weight%, the agglomeration of MnO_2 becomes visible as shown in SEM image Figure 4.2(c).

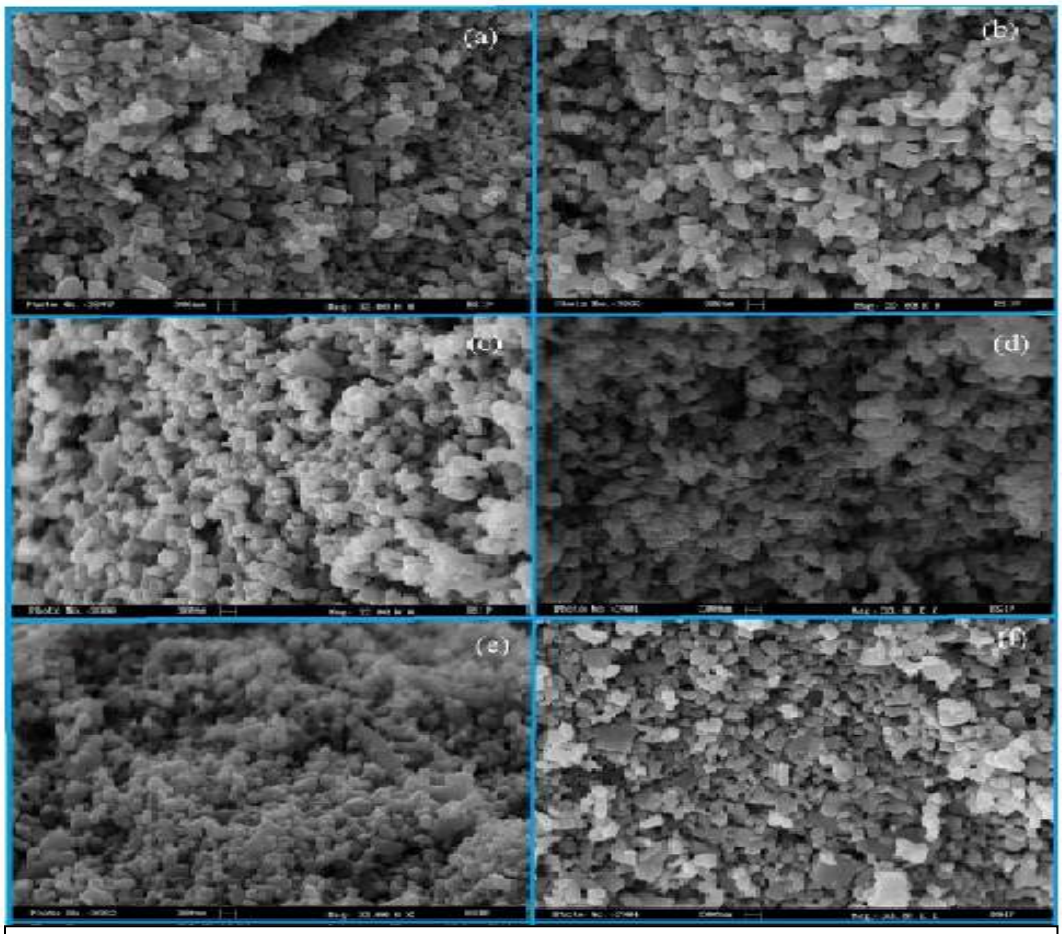

Figure 4.2 Surface microstructure of ZnO and ZnO-MnO_2 composite at 600^{o}C, (a) Pure ZnO, (b) ZnO-0.2 weight % MnO_2 and (c) ZnO-0.4 weight % MnO_2 (d) ZnO-0.6 weight % MnO_2 (e) ZnO-0.8 weight % MnO_2 and (f) ZnO-1.0 weight % MnO_2.

This agglomeration may increase the conductivity which decreases resistance more rapidly with adsorption of moisture. With further increase of doping concentration from 0.4 weight% to 0.6 weight%, the crystallization of zinc oxide was found to be higher as compared to lower doping concentration of MnO_2. This increase in size and number of pores are helpful for sensing the

humidity (Figure 4.2d). The shape of crystallite also changes from hexagonal to rectangular shaped crystallites. As shown in Figure 4.2(e) at 0.8 weight% doping of MnO_2 in zinc oxide, the shape of crystallites becomes mixed of spherical and rectangular, the higher degree of pores is may be attributed in the sample to the distribution in grain size. The better crystallization is observed at this doping concentration of 1.0 weight% of MnO_2, as reflected in Figure 4.2(f). The grain size for a fixed percentage of doping decreased when annealing temperature was increased. When annealing temperature was increased from 500°C to 600°C the grain size for 0.2% doping from 268 nm to 218 nm, for 0.4% doping from 251 nm to 208 nm, for 0.6% doping from 228 nm to 198 nm and for 1.0% doping from 223 nm to 192 nm. However, no definite trend was observed in the grain size measurement from SEM when doping percentage was increased for fixed annealing temperature.

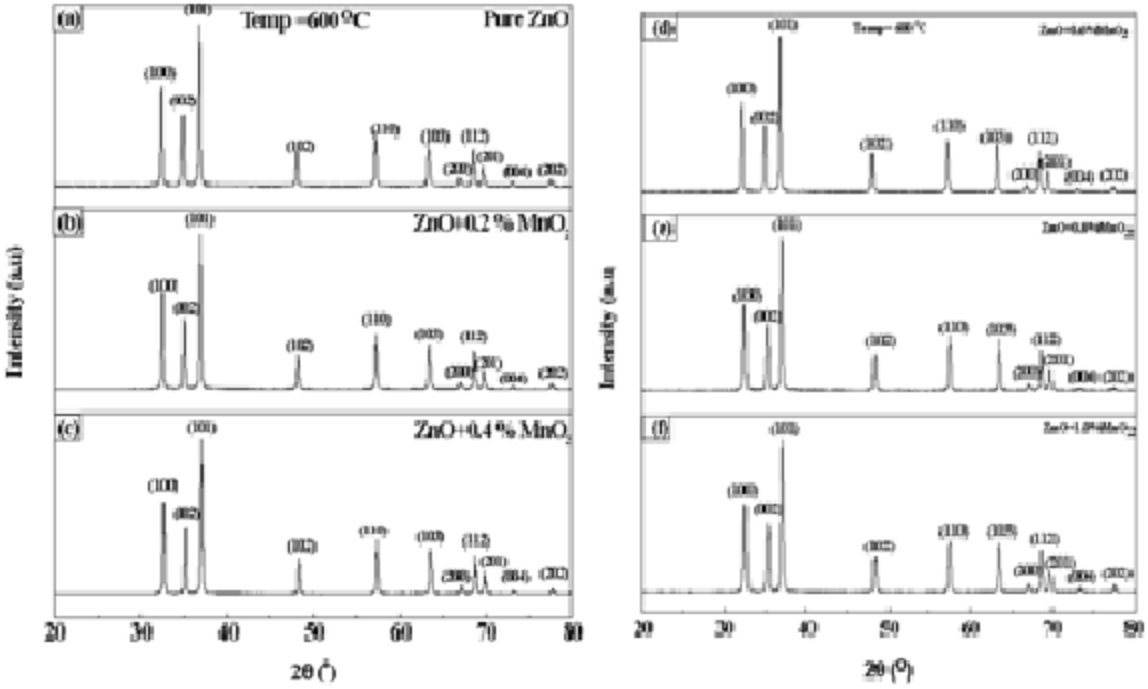

Figure 4.3 XRD Pattern of ZnO and ZnO-MnO_2 Composite in scanning range 20°-80° annealed at 600°C, (a) Pure ZnO, (b) ZnO-0.2 weight % MnO_2 and (c) ZnO-0.4 weight % MnO_2. (d) ZnO-0.6 weight % MnO_2 and, (e) ZnO-0.8 weight % MnO_2 and (f) ZnO-1.0 weight % MnO_2.

4.5 X-ray Diffraction

The average crystallite size of powdered samples were calculated by Debye-Scherer equation. The typical X-ray diffraction patterns of undoped and 0.2, 0.4, 0.6, 0.8, 1.0 weight% MnO_2 doped zinc oxide are shown in the Figure 4.3. These patterns are well matched with standard JCPDS file No. 79-2205. The results clearly indicate that the prominent peaks in the patterns correspond to hexagonal wurzite structure of zinc oxide. The crystallite sizes were found to be 49.7, 46.5, 43.3, 40.9, 35.0 and 31.7 nm for 0.0, 0.2, 0.4, 0.6, 0.8 and 1.0 weight% MnO_2 doped zinc oxide, respectively. The crystallite size decreased with increasing the concentration of MnO_2. The sharp intense peaks of ZnO confirms the good crystalline nature of ZnO and the diffraction peaks can be indexed to a hexagonal wurtzite structured ZnO; for

the MnO_2 doped ZnO the centres of all diffraction peaks have a slight shift compared to undoped sample.

4.6 Results and Discussion

The change in the value of resistance has been recorded with change in the %RH for different annealing temperatures. With change in %RH the fall in the value of resistance is very sharp; ranging from 200-300 MΩ to 0-10 MΩ over 10 to 99% RH. Hence, a graph between the logarithmic resistance value and %RH has been plotted. Figure 4.4 shows graphs for the pure ZnO, 0.4% MnO_2 doped ZnO and 1.0% MnO_2 doped ZnO, for the annealing temperature of 600˚C. Figure 4.4 also shows trend line of graphs for the 0.4% and 1.0% MnO_2 doped ZnO. Both of these trend lines match polynomial of degree 3 as depicted in the figure itself. The average sensitivity of the MnO_2 doped ZnO sensor increases with increase in the annealing temperature as well as the doping concentration of MnO_2. When annealing temperature is increased from 300˚C to 600˚C for pure ZnO the sensitivity increased from 2.1 MΩ/%RH To 3.4 MΩ/%RH. Similarily, when the annealing temperature is increased from 300˚C to 600˚C for 1.0% doped sample the sensitivity increased from 10.41 MΩ/%RH to 13.61 MΩ/%RH.

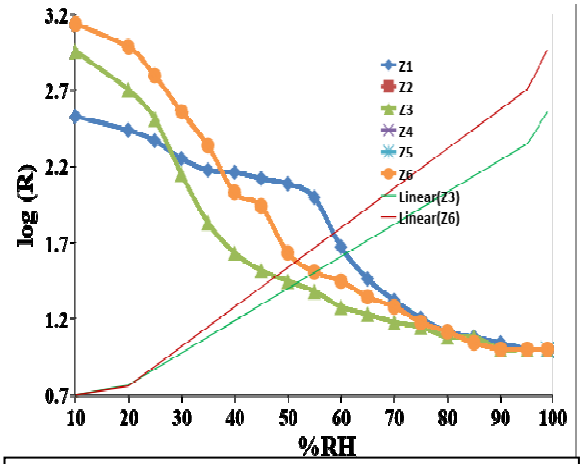

Figure 4.4 Logarithmic Plot of resistance values versus variation of % RH for sensing elements Z_1, Z_3, and Z_6.

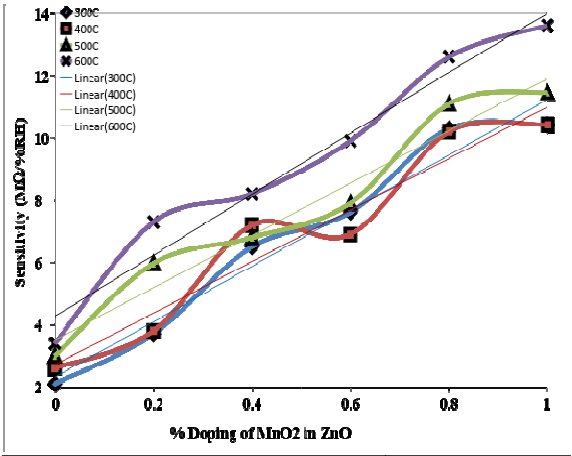

Figure 4.5 Change in sensitivity with change in annealing temperature and % doping of MnO_2 in ZnO.

Sensitivity increases with increase in the percentage of the doping. With increase in the concentration of MnO_2 the XRD peaks slightly shifted to higher Bragg angles compared to those for the pure ZnO sample. The diffraction angle for the ZnO peak [101] at 2-theta value of 35.1097 shifted to 35.2528 for 0.4 weight % MnO_2 doped ZnO and to 35.2844 for 1.0 weight % MnO_2 doped ZnO. Such changes are indeed expected if some of the Mn ions replace Zn ions in the lattice, as the Mn ions have smaller ionic radii [Mn^{4+} (0·056 nm) and Mn^{3+} (0·062 nm)] than Zn ions (0.74Å). The shift indicates decrease of lattice parameters. Some mechanisms were proposed to explain the surface conductivity change in the presence of watervapour. The surface first experiences the chemisorption of monolayer water with proton transfer among hydronium (H_3O+). Here, the electrical response depends on the number of water molecules adsorbed on the surface. The chemisorption is followed by physisorption of multilayer water with increase in humidity. Here, H_3O^+ appears in the physisorbed water and serves as a charge carrier. H^+ ions can move freely in the physisorbed water according to Grotthuss's chain reaction. At high humidity, electrolytic conduction replaces protonic conduction. Doping Mn ions into ZnO leads to higher charge density on the surface. In this case, a strong electric field is induced around the surface of Mn-doped ZnO. This

strong electric field augments ionization of water molecules and further affects the deeper physisorbed water. As the doping % increases more Mn ions get incorporated into ZnO lattice. This leads to higher charge density in the vicinity resulting in creation of a stronger electric field near the surface. When water vapours interact with the surface this high field causes ionization of water molecules leading to high conductivity. Thus the sensitivity increases with increase in concentration of MnO_2 in ZnO. Figure 4.5 shows graph for the change in the sensitivity of the samples both for the increase in the annealing temperature and the change in percentage of the MnO_2 in ZnO. A linear trend line is the best match for the sensitivity versus % RH graphs as shown in the figure for each annealing temperature. For annealing temperature 300˚C the sensitivity increases from 2.1 MΩ/%RH to 10.41 MΩ/%RH when the doping is increased from 0.0% to 1.0%. For annealing temperature 600˚C the sensitivity increases from 3.4 MΩ/%RH to 13.61 MΩ/%RH when the doping is increased from 0.0% to 1.0%. To determine the hysteresis effect in the sensing elements, the humidity in the chamber has been increased from 10% RH to 99% RH and then cycled down to 10% RH and the values of resistance of the sensing elements recorded with change in % RH. All sensing elements manifest acceptable hysteresis values in the range ±2% to ±5%, which is comparable to the commercial sensors. After the study of humidity sensing properties, sensing elements were kept in laboratory environment and the characteristics of humidity sensing were regularly monitored. For analyzing the effect of ageing, sensing properties of these elements were examined again in the humidity control chamber after six months and variation of resistance with % RH recorded and analyzed. For all the sensing elements annealed at 600°C, values were generally repeatable within ±2% in the 10%–99% RH range after six months. Response/recovery time is defined as the time taken to achieve 90% of the initial total resistance variation during the humidification and desiccation processes. As the annealing temperature increased the response/recovery time decreased. Response and recovery time for the sensing element of 1% MnO_2doopedZnO for the annealing temperature 600°C were 64 and 162 seconds, respectively. The response and recovery time for the sensing element of undopedZnO annealed at 600°C were 89 and 312 seconds, respectively.The undoped and MnO_2 doped nanostructured zinc oxide is successfully synthesized by solid state reaction route. X-ray diffraction study confirmed the formation of zinc oxide and its minimum average crystallite size was 47.5 nm. The doping of MnO_2 enhances the crystallization and decreases the crystallite size. The minimum average crystallite size was 31.7 nm for 1.0 weight% MnO_2 doped zinc oxide. Surface morphology of the sensing material showed the hexagonal shaped particles are uniformly distributed zinc oxide which leaves large number of pores. These pores act as humidity adsorption sites. With increase in the concentration of MnO_2 the pores increased. The optical band gap of the undoped zinc oxide was found to be 4.05 eV. The value of band gap decreases with increase in the MnO_2 doping concentration. The sensitivity increases with increase in annealing temperature. The sensitivity for the pure sample of ZnO increased from 2.1 MΩ/%RH to 3.4 MΩ/%RH when the annealing temperature was increased from 300 to 600ºC. For 1.0% MnO_2 in ZnO the sensitivity increased from 10.41 MΩ/%RH to 13.61 MΩ/%RH when the annealing temperature was increased from 300 to 600ºC. The sensitivity increased with increase in doping % of MnO_2 in ZnO. The sensitivity of undoped zinc oxide for the annealing temperature 600ºC was 3.4 MΩ/%RH whereas the sensitivity of the 1.0% MnO_2 doped ZnO was 13.62 MΩ/%RH for the same annealing temperature 600ºC. The hysteresis was within ±2 to ±5% and aging within ±2%. Response and recovery time for the sensing element of 1% MnO_2 doped ZnO for the annealing temperature 600°C were 64 and 162 seconds, respectively.

CHAPTER V

V_2O_5-ZnO Nanocomposite for Moisture Sensing Studies

5.1 Introduction

Inorganic compound Vanadium oxide (V_2O_5) is both an amphoteric oxide and an oxidizing agent. From the industrial perspective, it is the most important compound of vanadium, being principal precursor to alloys of vanadium and is a widely used industrial catalyst. In the present work, the sensing element V_2O_5 doped ZnO annealed at 500°C showed best results with sensitivity more than 350% higher than Cu_2O-ZnO and more than 700% times greater than Ag doped ZnO.V_2O_5-ZnO system exhibits multifunctional properties. Single phase V_2O_5-ZnO is considered as diluted magnetic semiconductor (DMS) material. Multi-phase ZnO–V_2O_5 manifests varistor like properties. While varistorproperties are generally due to greater metal ions but in ZnO–V_2O_5smaller vanadium ion is responsible.

5.2 Fabrication of Sensing Elements

Solid-state reaction route was adopted to fabricate nanocomposite samples of V_2O_5-ZnO. ZnO and V_2O_5 by different weight% were mixed. 10% by weight of glass powder (binder) was added. Mixers were grinded separately to uniformity. Samples with 0.2 %, 0.5%, 0.8%, 1.0% and 1.2% of V_2O_5inZnOwere labeled VZ-0.2, VZ-0.5, VZ-0.8, VZ-1 and VZ-1.2, respectively. Powders were pressed at room temperature into disc shaped pellets under 260 M Pa pressure. Pellet sample of pure ZnO was also fabricated for comparison purpose. Pellets were annealed in air at 500°C for 3 hours.

5.3 SEM and XRD Studies

Figure 1 and 2 show micrographs of pure ZnO and ZnO-V_2O_5nanocomposite samples. Micrographs show ZnO scattered throughout the whole substrate forming a network of voids and pores. SEM micrographs would reveal porous structure and small crystallites without inside pores but many inter grain pores. These pores are expected to provide sites for humidity adsorption. Higher porosity increases surface to volume ratio of the materials and therefore, helps in getting good sensitivity. The average grain size measured from SEM micrographs are 620 nm for sample of pure ZnO and 400 nm for ZnO-V_2O_5 nanocomposite sample. Figures 3 and 4 show XRD patterns for pure ZnO-V_2O_5nanocomposite.

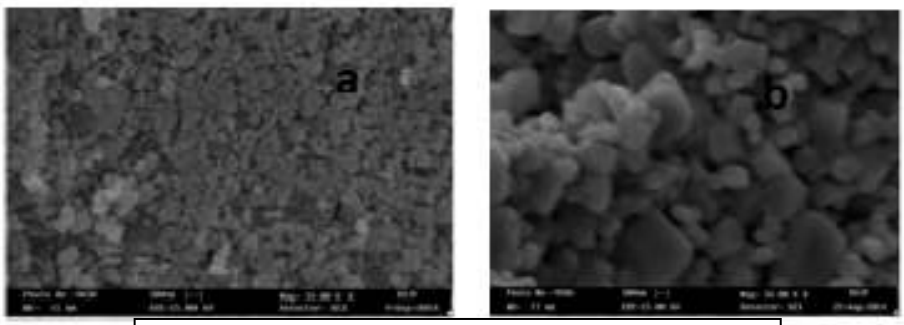

Figure 5.1 SEM of pure ZnO and V_2O_5 doped ZnO

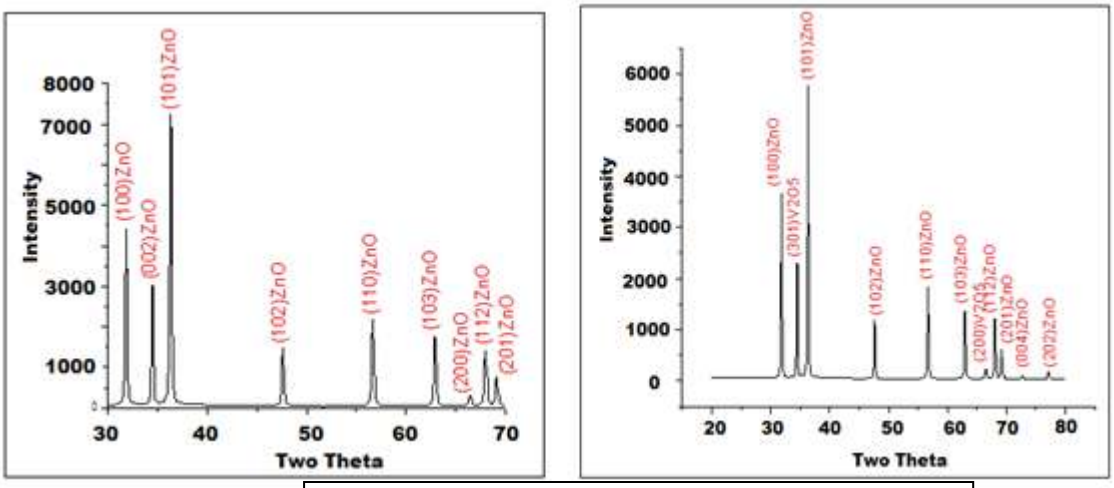

Figure 5.2 SEM of pure ZnO and V_2O_5 doped ZnO

5.4 Results and Discussion

Variation in resistance with change in %RH for V_2O_5-ZnO and pure ZnO samples for annealing temperature 500°C are plotted in Figure 5.3. A decrease in resistance is noticed with increase in the % RH for all samples VZ-0.0, VZ-0.2, VZ-0.5, VZ-0.8, VZ-1.0 and VZ-1.2. Fall is sharp for initial range of 35%-55% RH and gradual for 55%-95% RH range. Table 5.1 shows values of sensitivity for these samples; column I shows sensitivity for sample of pure ZnO. Column Ia indicates sensitivity for an initial increasing cycle, column Ib shows the sensitivity for decreasing cycle and Ic shows sensitivity value after six months for the sample of pure ZnO. Similar values of sensitivity for samples VZ-0.2, VZ-0.5, VZ-0.8, VZ-1.0 and VZ-1.2 are shown in columns II, III, IV, Vand of Table 5.1. With increase in doping percentage of V_2O_5 in ZnO the sensitivity of the pellet samples increased from 2.65 MΩ/%RH for pure ZnO to 16.88 MΩ/%RH for 1% V_2O_5 doped ZnO.

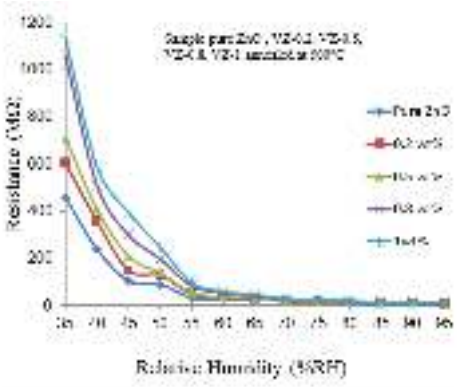

Figure 5.3 Resistance Vs %RH

Change in lattice parameters depends on ionic radius of doping atom. Doped atoms may substitute the Zn ion in the lattice. Use of additives arrests grain growth. When additive ions are smaller in size they comfortably take lattice sites. V^{5+} ions having much smaller size (63 pm) than Zn^{2+} (88 pm) are expected to take lattice site. Therefore, it is reasonable to suggest that most of V^{5+} takes lattice site. Ionic size of V^{2+} is 93 pm. In ZnO, due to charge matching, Zn^{2+} ions in lattice is generally substituted

by 2^+ oxidation state. For vanadium doping, ionic radius of V^{2+} (0.93 A˚) ion is larger than Zn^{2+} (0.88 A˚) ion. If V^{2+} ion substitutes Zn^{2+} ion in lattice then the ionic radii mismatch may cause change in lattice parameter. Some V^{2+} ions do substitute the Zn^{2+} ions in ZnO lattice leading to agglomeration and subsequent growth in grain size. This causes distribution of grain size leading to creation of more voids and porosity. Higher porosity increases surface to volume ratio. In this process, more surface area of sensing element gets exposed leading to more adsorption. This increases sensitivity. V_2O_5 behaves as acceptor impurity in n-type ZnO; hence, its presence in ZnO can modify electrical properties of ZnO and change its electrical response of ZnO.

Table 5.2 shows crystallite size at various 2θ values for pure ZnO and ZnO-V_2O_5nanocomposite. In case of pure ZnO sample there is distribution in size of crystallites. Minimum crystallite size is 447 nm at 2θ value of 31.82 and maximum 534 nm at 2θ value of 66.41. In case of ZnO-V_2O_5nanocomposite also a wide distribution in the size of crystallites is noticed. Minimum crystallite size occurring at 2θ value of 76.98 is 260 nm and maximum crystallite size occurring at 2θ value of 66.41 is 598 nm. Thus, in case of ZnO-V_2O_5nanocomposite, distribution in the crystallites size is as wide as 130% as compared to 20% in the case of pure ZnO sample. Hence, addition of V_2O_5 increases distribution of crystallite size. Addition of V_2O_5 also reduces average crystallite size. Average crystallite size for pure ZnO sample is 486 nm that reduces to 394 nm for ZnO-V_2O_5nanocomposite.

As V_2O_5 is doped in ZnO, an evolution in distribution of crystallite size is noticed. Grain size distribution is noticeably influenced by addition of V_2O_5 in ZnO. With increase in doping of V_2O_5 in ZnO, more pores and voids are created due to drift of V^{5+} ions in oxygen vacancies of ZnO during annealing process. Pure ZnO sample has relatively low adsorption capacity for moisture and hence low sensitivity due to uniform distribution of grains, less formation of voids; lower inter-connected voids or capillaries which are important conditions for adsorption of water molecules in the sample. Sensing element of ZnO-V_2O_5nanocomposite has higher void concentration and distribution of grain size. This synergy creates affinity towards moisture and thus higher conductivity. It is possible that multiplicative effect of two or more parameters of nanocomposite may cause higher sensitivity. The mechanism by which a metal atom interacts with the surface of a metal oxide is varied and complex, it is not easy to establish the exact single parameter affecting the sensitivity. Sample without V_2O_5 may have more grains per unit area of the surface, yet the range of crystallite or grain size distribution is so narrow and

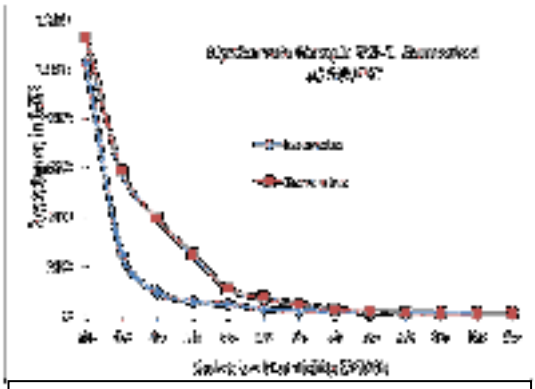

Figure 5.4 Hysteresis Graph for VZ-1

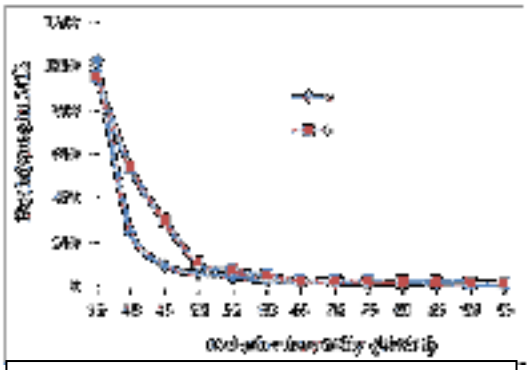

Figure 5.5 Aging Graph for VZ-1

limited (Table 5.2) that the surface of the composite appears smooth and therefore does not provide required porosity as adsorption sites.

Figure 5.4 shows hysteresis graph for sample VZ-1; the process of humdification and dehumidification together for VZ-1. Hysteresis can be minimized through the process of thermal desorption only. To estimate hysteresis, chamber humidity was scaled up from 35% RH to 95% RH and then cycled down to 35% RH. Samples show tolerable hysteresis values. Minimum hysteresis recorded for samples VZ-0.0, VZ-0.2, VZ-0.5, VZ-0.8 and VZ-1.0 were ±5.26, ±4.62, ±17.61, ±6.00 ±5.50 and±9.50, respectively. Figure 5.5 shows aging graph for the sample VZ-1. The graph shows an initial humidification process and humidification process after six months. Aging of sensors based on metal oxides is a significant retrograde. Data were found to be generally reproducible over different operation cycles. Sensitivity values were reproducible within ±5.28%, ±4.48%, ±3.85%, ±2.05%, ±1.48% and 2.95% for samples VZ-0.0, VZ-0.2, VZ-0.5, VZ-0.8, VZ-1.0 and VZ-1.2, respectively. As it is evident aging% decreased with increase in doping percentage of V_2O_5 in ZnO. Sample VZ-1 manifests reproducibility within ±2.0% which is quite high for sensors based on metal oxides. Figure 5.6 shows % hysteresis and % aging together for VZ-1with change in % of V_2O_5 in ZnO.

Figure 5.7 shows graph between sensitivity and % of V_2O_5 in ZnO for humidification, dehumidification and humidification after six months. The value of sensitivity increased with increase in % of V_2O_5 in ZnO up to 1% and after that the sensitivity did not increase. Thus the sensitivity is the maximum for VZ-1.0. The hysteresis is low for this sample at ±5.50 and the aging is only ±2.0.

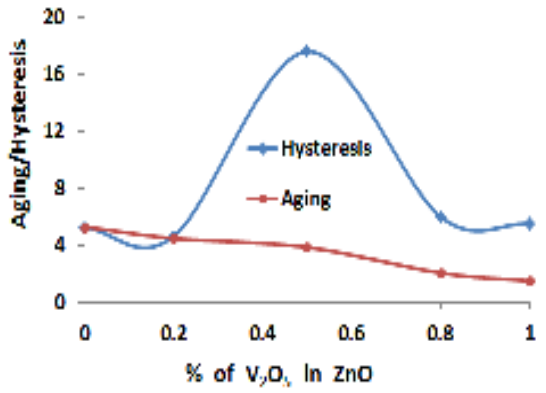

Figure 5.6 Aging & Hysteresis Vs % Doping

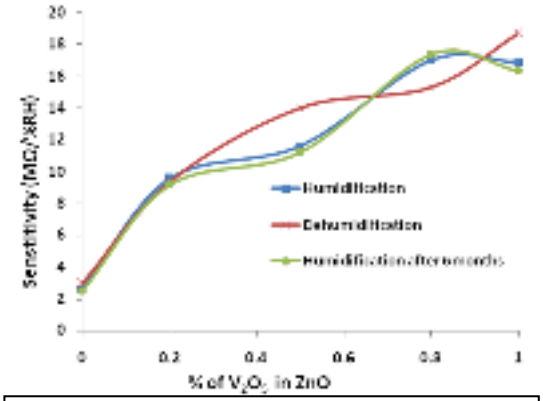

Figure 5,7 Sensitivity Vs % Doping

Sample VZ-1 shows best sensitivity of 16.88 MΩ%RH. For this sample, hysteresis is within ±6% and reproducibility within ±2% in 35-95% RH range. As % of V_2O_5 is increased in ZnO aging gets reduced from ±5.28 to ±1.48%. Grain size for sample of pure ZnO is 620 nm and for V_2O_5-ZnO nanocomposite 400 nm. As V_2O_5 in doped in ZnO there is an evolution in the distribution of crystallite size. Range of crystallite size for pure ZnO is 447-534 nm and for ZnO-V_2O_5 nanocomposite 260-598 nm. For ZnO-V_2O_5nanocomposite the distribution in the size of crystallites

is as wide as 130% as compared to only 20% in the case of pure ZnO sample. This results in the increase in sensitivity of ZnO-V_2O_5nanocomposite by more than 500% compared to the pure ZnO sample.

Table 5.1 Senstitivity of samples (MΩ/%RH)

I Sample Pure ZnO			II Sample VZ-0.2			III Sample VZ-0.5			IV Sample VZ-0.8			V Sample VZ-1.0		
a	b	c	a	b	c	a	b	c	a	b	c	a	b	c
2.65	2.95	2.51	9.58	9.4	9.15	11.66	14.05	11.21	17.01	15.33	17.36	16.88	18.71	16.63

[a]increasing cycle of relative humidity [b]decreasing cycle of relative humidity [C] increasing cycle alter six month

Table 2 Crystallite size variation with 2θ values

Sample of Pure ZnO		Sample of 1% ZnO-V_2O_5	
2θ	D (nm)	2θ	D (nm)
31.82	447	31.83	417
34.48	468	34.49	419
36.31	456	36.31	385
47.58	483	47.6	373
56.63	486	56.64	371
62.90	517	62.91	338
66.41	534	66.41	598
67.99	485	68.007	373
69.12	504	69.13	319
--	--	72.67	483
--	--	76.98	260

CHAPTER VI

Application of Undoped and Al_2O_3 doped ZnO Nanomaterials as a Solid-State Humidity Sensor and its Characterization Studies

This paper reports characterization and humidity sensing studies of pure ZnO and Al_2O_3 doped ZnO nanomaterials prepared by solid-state reaction route. Pellet samples of ZnO-Al_2O_3 nanocrystalline powders with 0, 3, 5, 10, 15 and 20 weight% of Al_2O_3 in ZnO were prepared. Prepared powders were given pellet shape under pressure of 260 M Pa and annealed at temperatures from 400°C to 700°C. When samples have been exposed to humidity, resistance of the pellet decreased with increase in relative humidity (RH) for the entire range of humidity from 10 % to 90 % RH range. The sample with 15 weight% of Al_2O_3 doped in ZnO and annealed at 700°C showed the best results with sensitivity of 14.98 MΩ/%RH. For this sensing element the repeatability over different cyclic operations is within ±2.00% of the measured values of sensitivity after six months. The response and recovery time of sensing element AZ-15 is found to be 85 seconds and 286 seconds, respectively. This sensing element manifests lower hysteresis, less effect of ageing and high reproducibility for annealing temperature 700°C. XRD pattern of this sensing element showed peaks of cubic gahnite and hexagonal corundum. Crystallite size for the sensing element of pure ZnO and Al_2O_3 doped ZnO are in 18–96 nm and 23–98 nm range, respectively. The average grain size for pure ZnO is 110 nm and for Al_2O_3 doped ZnO it is 114 nm, suggesting agglomeration of the crystallites in the sensing element to form larger grains.

6.1 Sample Preparation

The samples of ZnO-Al_2O_3 nanomaterials have been prepared through the solid-state reaction route. The starting material is ZnO (Qualizen, 99.99% pure). Thereafter, 3, 5, 10, 15 and 20 weight% of Al_2O_3 has been added to ZnO. 10 wt% of the ethyl cellulose is used as the binder. Thereafter, these powders have been mixed uniformly and these are made fine by grinding in the mortar with the pestle for 4 hours. The resultant powder for every doping percentage have were pressed into the pellet shape under pressure of 260 MPa in a hydraulic pressure machine (M.B. Instruments, Delhi, India) at 27 °C (room temperature). The pellet samples prepared are in the disc shape having a diameter of 12 mm and thickness 2 mm. After that the pressed powder pellets were annealed in air at temperatures 400 °C to 700 °C for 3 hours in an electric muffle furnace (Ambassador, India). The pellet samples made are AZ-0 (0 wt% of Al_2O_3 added to ZnO), AZ-3 (3 wt% of Al_2O_3 added to ZnO), AZ-5 (5 wt% of Al_2O_3 added to ZnO), AZ-10 (10 wt% of Al_2O_3 added to ZnO), AZ-15 (15 wt% of Al_2O_3 added to ZnO) and AZ-20 (20 wt% of Al_2O_3 added to ZnO). The pellet samples for pure ZnO (sample named as Z) were also prepared in the similar manner.

6.2 Scanning Electron Microscope Study

Figure 1 shows SEM micrographs of sensing elements of pure ZnO (sample Z) and Al_2O_3 doped ZnO (sample AZ-15) prepared through solid-state reaction route and annealed at temperature 700 °C. Micrographs show grains of ZnO scattered throughout the whole substrate forming a network of

pores and flakes. These pores are expected to provide sites for humidity adsorption. SEM micrographs (Figure 1b) reveal that as the temperature increases the porosity of the material increases forming clusters for Al_2O_3 doped in ZnO. The SEM micrographs show that the porous structure is dependent on the composition. Each composition is characterized by a typical porous structure and small crystallites without inside pores but many inter grain pores. In addition, one can observe that the intergranular pores are linked through the large pores. The pore structures should be regarded as interconnected voids that form a kind of capillary tubes. This structure favors the adsorption and condensation of water vapors. An observation of the crystallite size and grain size would suggest that smaller crystallites are getting agglomerated to form larger grains. In this process, more of the surface area of the sensing elements is exposed leading to more adsorption of water molecules. This increases the sensitivity of the sensing elements. The grain size calculated from SEM micrograph for sensing elements AZ-3, AZ-5, AZ-10, AZ-15, and AZ-20 are shown in Table 6.1. The average grain size for the sensing elements of pure ZnO and Al_2O_3 doped ZnO calculated from SEM micrographs are 110 nm and 114 nm, respectively. SEM micrographs show that the sensing elements manifest porous structure having granulation and tendency to agglomerate.

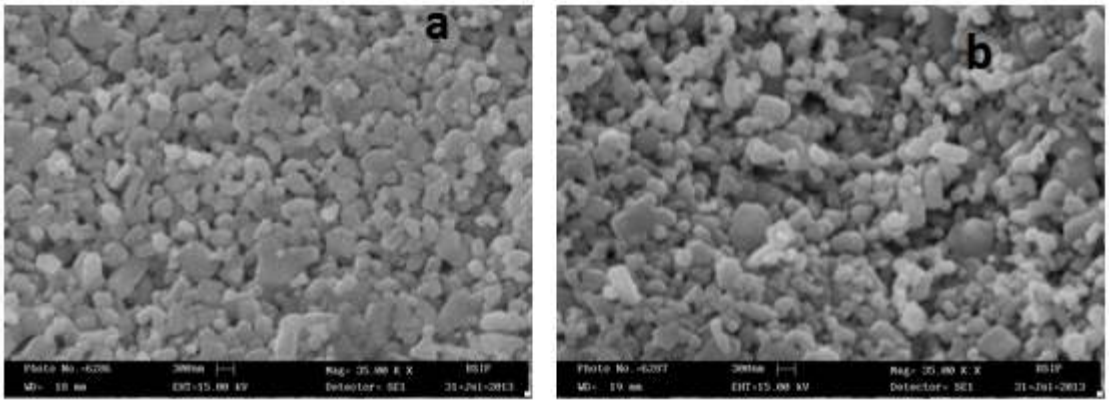

Fig.1. SEM Micrographs for Annealing 700°C, a. AZ-0; b. AZ-15

6.3. X-Ray Diffraction Analysis

Figure 6.2 shows X-ray pattern for the sensing element AZ-15 and AZ-0 annealed at 700°C. The pattern shows extent of crystallization of the sensing element in the form of powder. XRD pattern of AZ-15 shows peaks of cubic gahnite and hexagonal corundum. The crystallite size for the sensing element of pure ZnO is in the range of 18–96 nm. For the sensing element of Al_2O_3 doped ZnO, the range of crystallite size is 23–98 nm.

6.4. RESULTS AND DISCUSSION

Variation in resistance with the change in relative humidity has been recorded for all the sensing elements for different annealing temperatures from 400°C-700°C. All the results have been found to be repeatable. Variation in resistance with the change in relative humidity for AZ-3, AZ-5, AZ-10, AZ-15 and AZ-20 sensing elements for annealing temperature 700 °C has been shown in Figure 6.3 (dehumidification process) and Figure 6.4 (humidification process)..

All sensing elements have acceptable hysteresis values. Hysteresis is found to decrease with increase in the annealing temperature for sensing element AZ-0; the values of hysteresis being 4.80%, 4.30%, 3.50%, and 1.89% for annealing temperatures 400 °C, 500 °C, 600 °C, and 700 °C, respectively. For the sensing element AZ-15 the hysteresis values are 3.71%, 3.20%, 2.68%, and 1.26% for the annealing temperature 400 °C, 500 °C, 600 °C and 700 °C, respectively. Thus, there is a definite decrease in the hysteresis when Al_2O_3 is doped in ZnO. The data sheets of some commercially available humidity sensors have indicated hysteresis values in the range from 1.20%–5.00%. The sensing element AZ-15 annealed at 700°C shows lowest hysteresis value within acceptable limits.

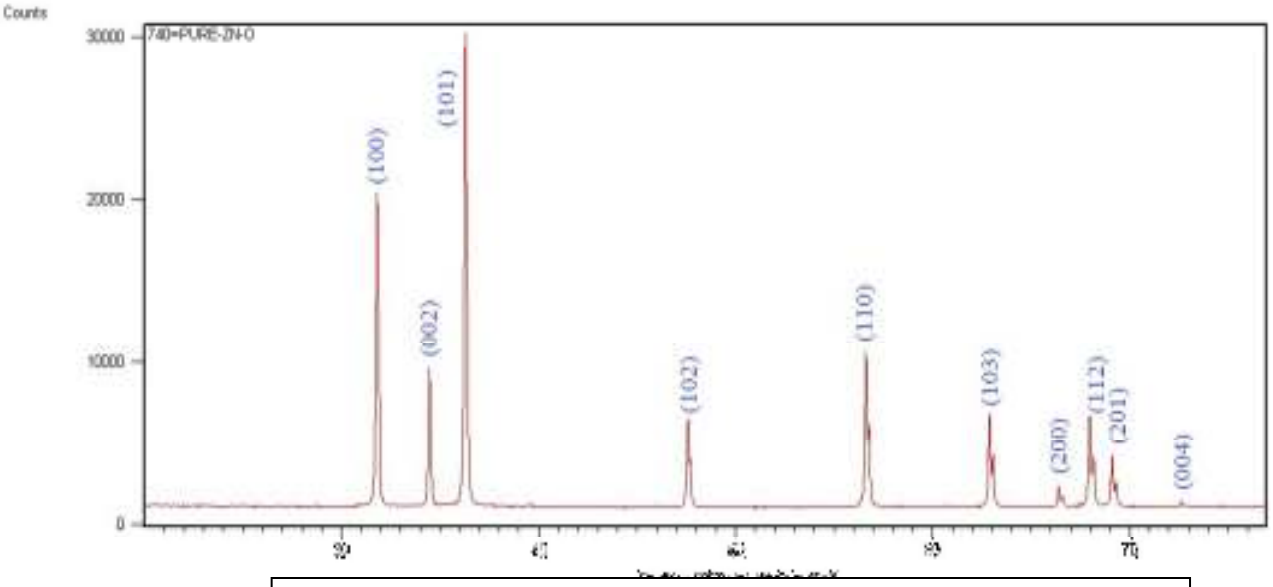

Figure 6.2. XRD of sample AZ-15 and AZ-0 for annealing annealed 700°C.

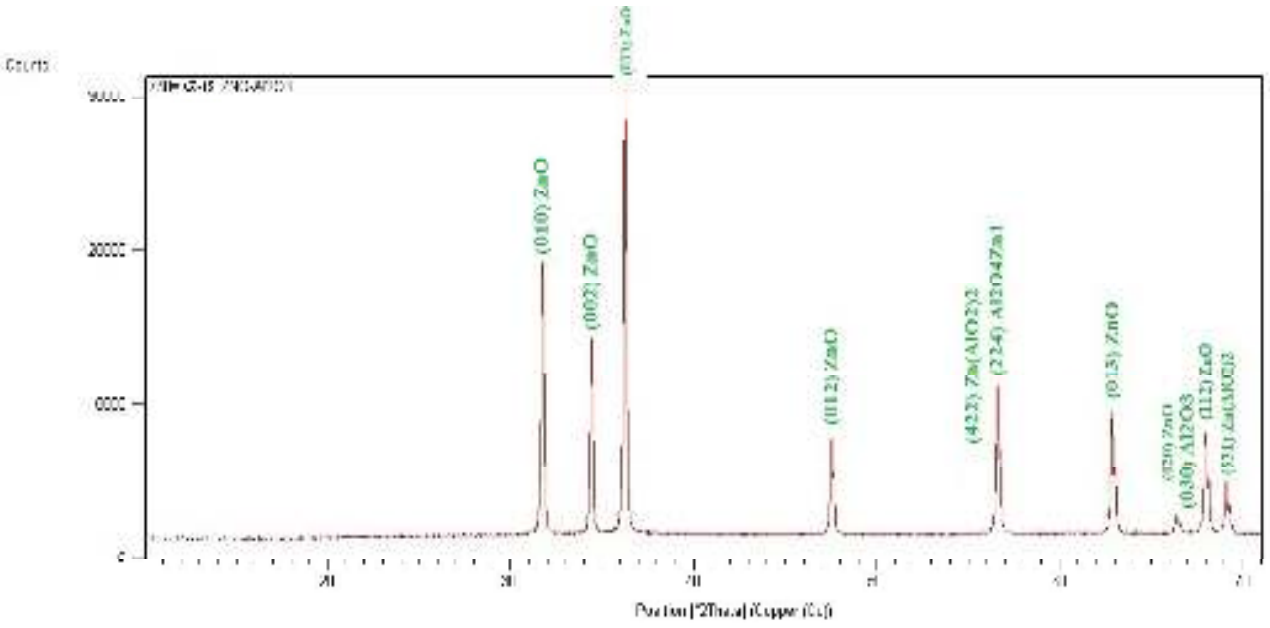

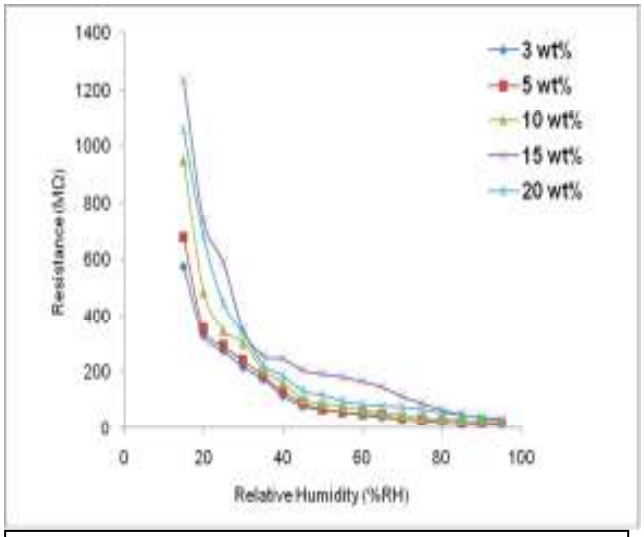

Figure 6.3 Resistance Vs Relative Humidity

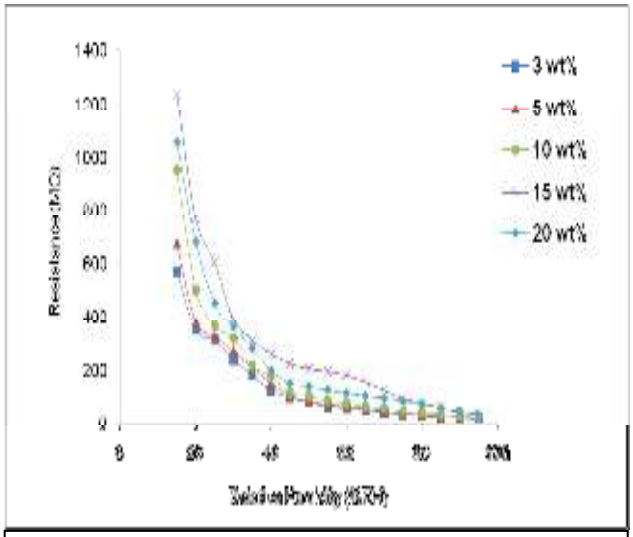

Figure 6.4 Resistance Vs Relative Humidity

For all the sensing elements annealed at 700°C, the values are generally repeatable within ±1.70% in the 10%–90% RH range after six months. All the sensing elements show significantly less ageing effect in their performance for all the annealing temperatures considered. We observe that the sensing elements both of pure ZnO (sample Z) and Al_2O_3 doped ZnO (sample AZ) show significantly less ageing effect in their performance for all the annealing temperatures considered.

The sensitivity values for the sensing elements AZ-3, AZ-5, AZ-10, AZ-15 and AZ-20 annealed at 700°C generally show that the sensitivity value increases with the increase in the doping percentage. The best sensitivity value is 14.98 MΩ/%RH for the sample AZ-15 annealed at 700°C. The sensitivity of this sample is highest among all samples because surface to volume ratio of the grains in this case has increased a lot which, in turn, provides more sites for water vapor to be adsorbed on the surface of the sensing element. For sensing element AZ-15 annealed at 700°C, the sensitivity is found to be repeatable within ±2.00% in dehumidification cycle of relative humidity and within ±1.5% over humidification cycle of relative humidity after six months. For pure ZnO sensing element annealed at 700°C the sensitivity value is 12.35 MΩ/%RH. Sensitivity increases with the increasing annealing temperature. With increase in the annealing temperature the grain size generally decreases. This leads to increase in surface to volume ratio. Thus, more of the surface area is exposed for adsorption, leading to higher sensitivity. Sensitivity values for all the sensing elements (AZ) for different annealing temperatures have been calculated and shown in Table 6.2. The sensitivity values for all pure (undoped) ZnO sensing elements (Z) for different annealing temperatures have been calculated and shown in Table 6.3.

Response/recovery time for the sensing element Z (pure ZnO) for the annealing temperatures 400°C, 500°C, 600°C, and 700°C are 130/680, 115/625, 96/350, and 91/315 seconds respectively. Response/recovery time for the sensing element AZ-15 for the annealing temperatures 400°C,

500°C, 600°C, and 700°C are 118/360, 106/340, 98/310, and 85/286 seconds, respectively. Since desorption is an endothermic process, it takes longer time to desorb the water vapor; therefore, the recovery time is always greater than the response time.

6.5 Regression Analysis

A polynomial of fourth degree fitted to the curve of sensitivity versus % doping of Al_2O_3 in ZnO.

$$y = -0.000x^4 + 0.012x^3 - 0.125x^2 + 1.117x + 4.369$$

Here, x= % doping of Al_2O_3 in ZnO and y= Sensitivity in MΩ/%RH (6.1)

We have also found that a polynomial of third degree fitted to the curve of sensitivity versus temperature graph of the sensing element AZ-15.

$$y = 2E\text{-}08x^3 - 3E\text{-}05x^2 + 0.020x + 10.48 \quad (6.2)$$

Here, x= Temperature and y= Sensitivity in MΩ/%RH

Also, for the undoped ZnO we have found that a polynomial of third degree fitted to the curve of sensitivity versus temperature graph.

$$y = -3E\text{-}07x^3 + 0.000x^2 - 0.214x + 41.86 \quad (6.3)$$

Here, x= Temperature and y= Sensitivity in MΩ/%RH

A regression analysis of the humidification graphs of undoped and Al_2O_3 doped ZnO was also carried out. Least square fit with respect to the polynomials of fifth degree were established. The coefficients of the various powers of x (%RH) with respect to y (Resistance) are tabulated in Table 6.5 (coefficients of a fifth degree polynomial). It can be observed from the tables that a_1, the coefficients of the first power of x in the polynomial is the dominant one, indicating a strong linearity between x and y i.e., RH and Resistance. Due to the advancement in the instrumentation technology, it is not essential to go for a linear response in sensors; a single valued function will be sufficient.

TABLE 6.1 Grain Size (nm)

AZ-3	AZ-5	AZ-10	AZ-15	AZ-20
98	110	118	114	120

TABLE 6.2 Sensitivity of Samples (MΩ/%RH

Temp. (ºC)	Sample (AZ-3)			Sample (AZ-5)			Sample (AZ-10)			Sample (AZ-15)			Sample (AZ-20)		
	a	b	c	a	b	c	a	b	c	a	b	c	a	b	c
400 ºC	6.14	6.80	6.13	7.13	7.87	7.11	10.79	11.04	10.76	14.48	14.63	14.45	12.38	12.68	12.35
500 ºC	6.35	6.84	6.33	7.29	7.98	7.26	10.85	11.14	10.82	14.68	14.74	14.65	12.50	12.65	12.46
600 ºC	6.60	6.86	6.56	7.35	8.04	7.32	10.98	11.29	10.96	14.80	14.85	14.77	12.71	12.74	12.68
700 ºC	6.90	6.99	6.85	8.14	8.23	8.12	11.54	11.63	11.51	14.96	14.99	14.93	12.78	12.85	12.75

[a] Increasing cycle of relative humidity; [b] Decreasing cycle of relative humidity; [c] Increasing cycle after six months

TABLE 6.3 Sensitivity of Samples of Undoped ZnO

Annealing Temperature	Sensitivity (MΩ/%RH) (Undoped ZnO)		
	a	b	c
400 ºC	8.18	8.56	8.16
500 ºC	9.41	9.89	9.38
600 ºC	11.30	11.88	11.28
700 ºC	12.25	12.45	12.23

[a] Increasing cycle of relative humidity; [b] Decreasing cycle of relative humidity; [c] Increasing cycle after six months

TABLE 6.4 Hysteresis of Samples of Undoped and Doped ZnO

Annealing Temperature	Hysteresis of Undoped ZnO	Hysteresis of sensing element AZ-15
400 ºC	4.80%	3.71%
500 ºC	4.30%	3.20%
600 ºC	3.50%	2.68%
700 ºC	1.89%	1.26%

TABLE 6.5 Coefficients of Various Powers of x for Polynomial of Degree 5

	Polynomial Coefficients					
Samples	a_o	a_1	a_2	a_3	a_4	a_5
AZ-3	1486	- 95.65	2.809	- 0.043	0.000	-1×10^{-06}
AZ-5	2032	- 150.4	4.985	- 0.084	0.000	-2×10^{-06}
AZ-10	3515	- 290.3	10.1	- 0.174	0.001	-5×10^{-06}
AZ-15	3889	- 280.3	8.554	- 0.128	0.000	-3×10^{-06}
AZ-20	3313	- 239.4	7.423	- 0.116	0.000	-3×10^{-06}
Undoped ZnO	178.2	111.9	- 6.019	0.123	- 0.001	4×10^{-06}

x (Relative Humidity); y (resistance of the samples); data fitted to a polynomial of degree
$y=a_0+a_1x+a_2x^2+a_3x^3+a_4x^4+a_5x^5$

CHAPTER VII

Nanostructured Undoped and Cu-doped ZnO Thin Films as Gas Sensor

In this chapter analysis on gas sensing application of undoped and Cu-doped ZnO nanostructured materials has been reported. Undoped and Cu-doped ZnO thin films were prepared for sensing studies. Undoped and Cu-doped ZnO thin films annealed at 600ºC showed the best results with sensitivity of 500 (%) and 724 (%), respectively in the 500-5000 ppm range. Other parameters like response time, recovery time, hysteresis and ageing effects were also studied. For the sensing element of 7 at% Cu doped in ZnO the range of crystallite size is 25-41 nm. The crystallite size for the sensing element of undoped ZnO annealed at 600°C is in the 24-38 nmrange. The average grain size as measured from SEM micrograph for 7 at% Cu doped in ZnO and undoped ZnO sensing elements were 36 nm and 42 nm respectively.

7.1 Introduction

The gas sensors based on the semiconducting metal-oxides such as SnO_2 and ZnO [7-10] were found to be very useful for detecting the toxic gases. A gas sensor must possess at least two functions, that is, to recognize a particular gas and to transduce the gas recognition into measurable sensing signals. Semiconductor gas sensors are solid-state sensors whose sensing component is made up of mostly semiconductor metal oxide. The development of semiconducting metal oxides as gas sensors has accelerated over the past 25 years. It has been well known that absorption or desorption of a gas on the surface of a metal oxide changes the conductivity of the material. The metal oxide semiconductor sensors have a large effective surface area, so as to adsorb as much of the target analyte as possible on the surface, giving a stronger and more measurable response (especially at low concentrations). The report on a ZnO-based thin film gas sensor gave rise to extraordinary development and commercialization of a host of semiconducting oxide for the recognition of a variety of gases over a wide range of composition. ZnO is sensitive to many gases of interest like hydrocarbons, H_2, oxygen H_2O, CO, NO_2 [14-19] etc., and has satisfactory stability over a wide range of temperatures (20 ^{0}C to 35 ^{0}C). Basic requirement for the sensor is its change in electrical conductivity with exposure of LPG to semiconducting oxides which depends on their band gaps, surface morphology, size, diffusion rate of gas and specific surface area [20]. Liquefied Petroleum Gas (also called LPG, GPL and LP) is a mixture of hydrocarbon gases used as fuel in heating appliances and vehicles. It is a low carbon-emitting hydrocarbon fuel available in rural areas, emitting 81% of the CO_2 per KWh produced by oil, 70% of that of coal, and less than 50% of that emitted by coal-generated electricity distributed via the grid. LPG has a typical specific calorific value of 46.1 MJ/Kg compared with 42.5 MJ/Kg for fuel-oil and 43.5 MJ/Kg for premium grade petrol (gasoline) [21]. Liquefied Petroleum Gas is widely used as a fuel for industrial and domestic purposes, has often proved to be hazardous because of explosions caused by leaks. The development of gas sensors in particular combustible gases is imperative due to the concern for safety requirements in homes and for industry. Specially, the liquefied petroleum gas (LPG), which is one of the mostly used but potentially hazardous gas, because explosion accident may be caused when it

leaks out accidentally or by mistake. Gas leakage tragedies and accidents have led to heavy losses over the years. So it is very important to detect any gas leakage and prevent any accidents. Because the sensing phenomenon generally takes place on the surface of sensing element, hence the surface morphology has an essential role on the sensitivity of sensor. Among the structural parameters, the crystallite size has prominent effect on the gas sensitivity. This chapter reports gas sensing properties of nanostructured pure zinc oxide (ZnO) [22-27].

Arindam Ghosh et al. [28] reported work on the low temperature LPG sensing properties of wet chemically grown zinc oxide nanoparticle thin film and found higher sensitivity towards liquefied petroleum gas (LPG) at optimized temperature of∼200 °C. The response and recovery times with 200 ppm of LPG were found to be 6 and 8 s, respectively. Maximum response of 59% was achieved by AarthySivapunniyam and his co-worker [29] for 9000 ppm LPG at 250 ℃ towards highly sensitive zinc oxide (ZnO) nanorods based gas sensors. They also reported higher response of 63% for 3000 ppm LPG at 250 °C when the surface of ZnOnanorods was modified using zinc stannate (Zn_2SnO_4) microcubes. P. P. Sahay et al. [30] reported the maximum response (89%) to 1 vol% of LPG in air at 325°C and shorter response and recovery times of the 0.5 at % Al-doped ZnO film prepared by chemical spray pyrolysis technique using $Zn(CH_3COO)_2$ as a precursor solution with $AlCl_3$ as a doping solution. L. A. Patil et al. [31] reported work on ultrasonically prepared nanocrystallineZnO thin films. They found that the films fired at 500 °C are highly sensitive to LPG at 300 °C. Tanushree Sen et al. [32] studied and found the excellent sensing ability of **Polyaniline/γ-ferric oxide (PANi/γ-**Fe_2O_3) nanocomposite films toward LPG of 50–200 ppm concentrations at room temperature. The nanoscale morphology of the composites provided a large surface area for the adsorption of gas molecules, thus enhancing the gas sensitivity. The sensing mechanism pertains to a change in the depletion region of the p–n **junction formed between PANi and γ-**Fe_2O_3as a result of electronic charge transfer between the gas molecules and the sensor. The maximum response was obtained for **PANi/γ-**Fe_2O_3(3 wt%) nanocomposite for 200 ppm LPG. The response times of these sensors were found to be as low as 60 s. K. V. Gurav group [33] reported the work on LPG sensing properties of Pd-sensitized one-dimensional (1-D) vertically aligned ZnOnanorods synthesized on glass substrate through a simple chemical route. The morphology and structure of vertically aligned ZnOnanorods has been characterized by scanning electron microscopy (SEM) and X-ray diffraction (XRD) analysis. The LPG sensing properties of the vertically aligned ZnOnanorods are improved significantly after palladium (Pd) sensitization. The unsensitized vertically aligned ZnOnanorods exhibited the maximum response of 37% at 573 K upon exposure to 2600 ppm LPG, which improved to 60% at operating temperature of 498 K after the Pd sensitization. The Pd-sensitized vertically aligned ZnOnanorods showed more selectivity towards LPG as compared to CO_2. Their results demonstrate that the chemically grown vertically aligned ZnOnanorods along with Pd sensitization are promising material for the fabrication of cost effective and high performance gas sensors. NanocrystallineZnO films were deposited onto glass substrates by spray pyrolysis of zinc nitrate solutions and used as a liquid petroleum gas (LPG) sensor by V. R. Shinde and his team [34]. The dependence of the LPG sensing properties on the molar concentration of zinc nitrate solutions was investigated. The ZnO films were oriented along with the hexagonal crystal structure. The grain size and grain density increased with an increase in molar concentration of zinc nitrate solutions. The gas sensing properties for LPG of the ZnO films for LPG with different grain sizes were measured at different temperatures. The maximum sensitivity of 43% at

the operation temperature of 673 K was found for the ZnO film prepared by spraying a 0.1 M solution. The ZnO thin films exhibited good sensitivity and rapid response–recovery characteristics to LPG. Further, it has been shown the gas sensitivity of the ZnO gas sensor depends upon its grain size.

Liquefied petroleum gas (LPG) is flammable mixture of hydrocarbon gases used as fuel in heating appliances, cooking equipment, vehicles, etc. Liquefied petroleum gas is also referred to as simply propane or butane or even mixture including both propane and butane. So, the development of LPG sensors is an important aspect. Various types of gas sensing materials have already been investigated by different researchers in the entire world [35-40]. The metal oxide nanomaterials including nanoparticles, nanorods, nanowires, quantum dots, nanotubes and thin films have attracted much attention in the entire world due to their fascinating novel properties. Metal oxides like zinc oxide (ZnO) have various applications in gas and humidity sensing[41-51]. Synthesis methods play very important role to control the size and surface area of materials. Thick and thin film based gas sensors are getting more and more attention for attaining enhanced sensitivity parameters [52-54].

7.2 Gas Sensing Mechanism

When the sensing elements come in contact with air then various types of oxygen ionic species (e.g. O^{2-}, O_2^{2-}, O_2^{-}) are formed at the surface of thin film. Adsorption of oxygen molecules play significant role in the resistance of thin films. The probability of formation of high or low amount of chemisorbed oxygen ion species depends on temperature. During the interaction of the LPG molecules with the surface of the thin film the following chemical reactions may occur:

$$C_nH_{2n+2} + O_2^{2-} \rightarrow C_nH_{2n-2} + 2H_2O + 2e^-$$
$$C_nH_{2n+2} + O_2^{2-} \rightarrow C_nH_{2n}O + H_2O + 2e^-$$
$$C_nH_{2n+2} + O_2^{-} \rightarrow C_nH_{2n-2} + 2H_2O + e^-$$
$$C_nH_{2n+2} + O_2^{-} \rightarrow C_nH_{2n}O + H_2O + e^-$$
$$C_nH_{2n+2} + O^{2-} \rightarrow C_nH_{2n} + H_2O + 2e^-$$
$$C_nH_{2n+2} + 2O^{2-} \rightarrow C_nH_{2n}O + H_2O + 4e^-$$

Here, C_nH_{2n+2}represents various types of hydrocarbons (e.g. butane, propane, methane, etc.). From the above chemical reactions it is clear that the reaction is taking place between LPG molecules and chemisorbed oxygen ionic species. The chemical reactions that occur due to the interaction of LPG molecules with the nanostructured material are complex and depend on the operating temperature of the sensing elements also. Different chemical reactions yield different nanostructures and hence different surface morphology. Moreover, chemical reactions are controlled by chemical kinetics. The chemical kinetics depends upon various factors like gas concentration (or pressure), temperature, etc. So, the chemical reactions also depend on these factors.

7.3 Device Assembly

For the LPG sensing measurements a special gas chamber was designed which consists of a gas inlet and an outlet knob for LPG exclusion. The schematic diagram of experimental setup is shown in figure 7.1. The sensing system comprising of a vacuum chamber with approx 6” dia and 8” tall with ports and tripod for table top mounting, a gas valve, isolation valve for pump along with a piraniguage for measuring pressure, included 1.5” dia heater capable of working up to 500°C in

vacuum as well as oxygen. The sensing system contains 8 isolated ports for probe connection with clips. The sensing pellet was inserted between the Ag electrodes inside the stainless steel chamber having inlet and outletknobs for LPG. A multi-meter (sinometer, ± .001M**Ω, Model: VC**-9808) was used to record the variation in resistance with change in pressure.

Figure 7.1 Gas Sensing Assembly

7.4 Results and Discussion

The sensitivity of a semiconductor gas sensor at a specific temperature is given by,

$$\text{Sensitivity}\ (\%) = \left(\frac{R_{air}}{R_{gas}}\right) \times 100$$

Here, R_{air} = Resistance of the sensing element (thin film) in air; R_{gas} = Resistance of the sensing element (thin film) in gas.

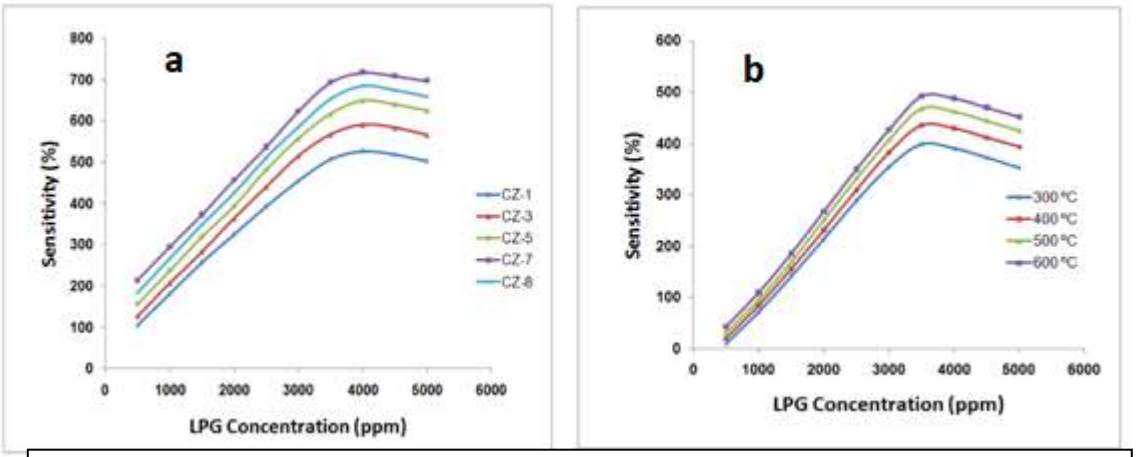

Figure 7.2 Sensitivity Vs LPG Concentration a. for samples CZ-1, CZ-3, CZ-5, CZ-7 and CZ-8 annealed at 600°C; b. for Sample CZ-0

An effort has been made, in the present research work, to develop an excellent sensor which could detect even a very small amount of leakage of LPG at room temperature (operating temperature). Sensitivity of Cu-doped ZnO thin films for all sensing elements for annealing temperatures 300°C–600°C are shown in Table 7.1. Sensitivity of undoped ZnO thin films for annealing temperatures 300°C–600°C are shown in Table 7.2. Figure 7.2(a) shows variation of sensitivity with change in gas concentration for the sensing elements CZ-0, CZ-1, CZ-3, CZ-5, CZ-7 and CZ-8 annealed at 600°C. Figure 7.2(b) shows variation of sensitivity with change in gas concentration for the sensing elements CZ-0 annealed at different temperatures. CZ-0 (undoped ZnO) and CZ-7 (Cu-doped ZnO) thin films annealed at 600ºC showed the best results with sensitivity of 500 (%) and 724 (%) respectively in the 500-5000 ppm range. Figure 7.2(a)

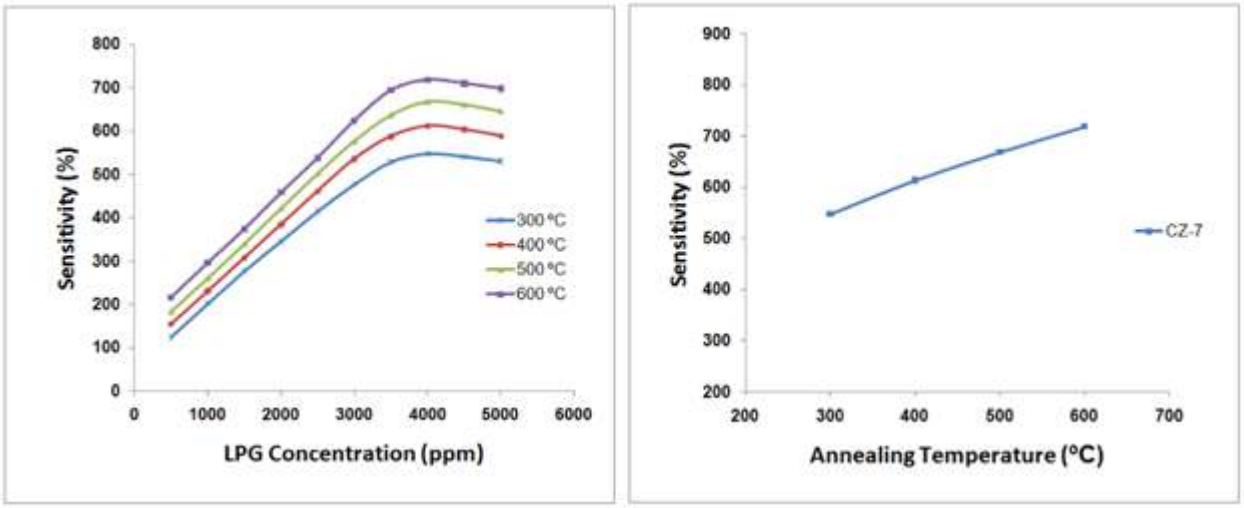

Figure 7.2 a. Sensitivity Vs Gas Concentration for CZ-7; b. Sensitivity Vs Annealing Temperature for CZ-7

shows variation of sensitivity with change in gas concentration for the sensing elements CZ-7 annealed at different temperatures.When an n-type semiconductor interacts with a reducing gas then the conductivity increases and hence resistance decreases. Cu doping enhances the electrical properties of the nanomaterials.With the increase in the gas concentration the pressure also increases which in turn increases the probability of interaction between the LPG molecules and the surface of the thin film and hence the chemical reaction rate increases. With the increase in the gas concentration the sensitivity increases. Moreover, Cu-doping enhances the adsorption and desorption rates of gas molecules which leads to increase in the sensitivity value. During the initial interaction between the LPG molecules and the thin film surface, the adsorption sites are gradually occupied by the LPG molecules. When the gas concentration level is considerably increased (i.e. beyond 4000 ppm for Cu-doped ZnO thin films and beyond 3500 ppm for undopedZnO thin films) then at this stage there are almost no more adsorption sites available to be occupied by the LPG molecules but with the increase in the gas concentration level the pressure increases and hence the chemical kinetics changes considerably. Due to considerable change in the chemical kinetics a large number of new chemical species (or swarm of new type of chemical species) are formed which leads to a slight decrease in the sensitivity. As a matter of fact a sudden formation of swarm of new chemical species,

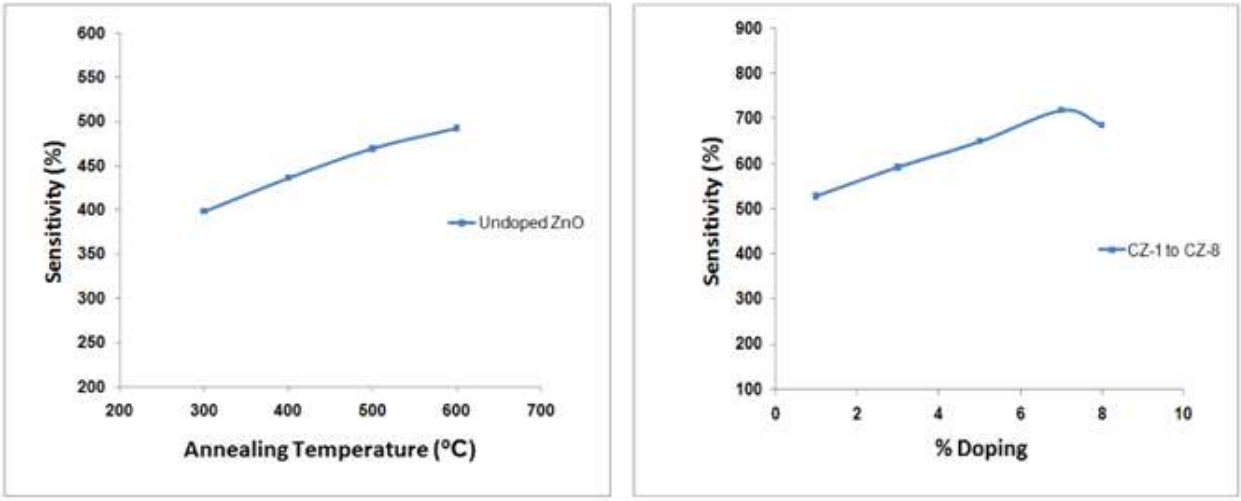

Figure 7.3 a. Sensitivity Vs Annealing temp for CZ-0; Sensitivity Vs % Doping for Annealing Temp 600°C

due to considerable change in the chemical kinetics, may result in either decrease (or increase) of sensitivity. Figure 7.3(b) shows variation of sensitivity with annealing temperature for the sensing elements CZ-7. Figure 7.3(a) shows variation of sensitivity with annealing temperature for the sensing elements CZ-0. From Figure 7.3b and Figure 7.3a it is clear that with the increase in the annealing temperature sensitivity increases. As a matter of fact with the increase in the annealing temperature the probability of formation of adsorption sites or porosity (or voids)increases due to which the adsorption and desorption rates of gas molecules increases which in turn increases the sensitivity. Figure 7.3(b) shows variation of sensitivity with % doping for Cu-doped ZnO sensing elements annealed at 600°C. For lower doping percentage of Cu in ZnO, most of Cu^{2+} takes lattice site for all the compositions thereby increasing grain size. The grain size is found to increase from 18 nm for CZ-1 to 45 nm for CZ-8. For higher compositions Cu^{2+} tends to segregate at the grain boundaries of host particles thus arresting particle growth. For higher doping compositions (above 7 at% doping) agglomeration of large number of crystallites occurs due to which the grain size is immensely increased which is responsible for decrease in the porosity of the sensing element. This leads to the decrease in the sensitivity of the sensing element. Due to this reason sensing element CZ-8 has lower sensitivity than sensing element CZ-7. The texture and grain size distribution are highly affected by increase in annealing temperature. More voids are created during the annealing process. Sensing element of CZ-7 annealed at 600°C has maximum void concentration and porosity. The sensitivity of sensing element CZ-7 is larger than the others. The surface morphology is an important aspect from sensitivity perspective. As the surface area increases, the probability of adsorption and desorption of gas molecules increase and hence the sensitivity increases.

Regression Analysis:

A regression analysis of the LPG sensing graphs of Cu-doped ZnO nanomaterial was carried out.

A polynomial of fourth degree (given below) fitted to the curve of sensitivity versus doping percentage graph of the sensing elements (CZ-1 to CZ-8) annealed at 600°C.

$$y = -0.732x^4 + 12.12x^3 - 67.45x^2 + 173.5x + 410.5 \qquad (7.1)$$

Here, x= %Doping and y= Sensitivity (%)

Moreover, it is also found that a polynomial of third degree (given below) fitted to the curve of sensitivity versus annealing temperature graph of the sensing element CZ-7.

$$y = 5E\text{-}07x^3 - 0.001x^2 + 1.2x + 268 \quad (7.2)$$

Here, x= Annealing Temperature and y= Sensitivity (%)

It is also found that a polynomial of third degree (given below) fitted to the curve of sensitivity versus annealing temperature graph of the sensing element CZ-0.

$$y = -8E\text{-}07x^3 + 0.000x^2 + 0.163x + 304 \quad (7.3)$$

Here, x= Annealing Temperature and y= Sensitivity (%)

Figure 7.4(a) shows hysteresis behavior of sample CZ-7 annealed at 600°C. Hysteresis phenomenon in metal oxide materials is mainly due to chemisorption and physisorption processes. To determine the hysteresis effect in the sensing elements, the LPG gas concentration in the chamber has been increased from 500 ppm to 5000 ppm and then cycled down to 500 ppm and the values of resistance of the sensing elements recorded with change in gas concentration. All sensing elements manifest acceptable hysteresis values. Hysteresis was found to decrease with increase in the annealing temperature for sensing elements of CZ-7 thin films; values of hysteresis being 4.18%, 3.32%, 2.25% and 1.64% for annealing temperatures 300°C, 400°C, 500°C and 600°C, respectively. For sensing element CZ-0, hysteresis values are 4.92%, 3.84%, 2.96% and 2.18% for annealing temperatures 300°C, 400°C, 500°C and 600°C, respectively. So, a decrease in the value of hysteresis was observed in the case of Cu-doped ZnO sensing element annealed at 600°C over that of undoped ZnO.As a matter of fact, the energy required for the removal of the physisorbed layer is very less in comparison to the energy required for the removal of chemisorbed layer. With increase in annealing temperature the porosity (as well as adsorption sites) of the developed thin films increases.Moreover, the thin film annealed at higher temperature hasthe high probability of adsorption and desorption of gas molecules at high rates. That is why hysteresis decreases with the increased annealing temperature. The sensing element annealed at 600°C shows lowest hysteresis value within acceptable limits. The nanomaterials formed provide enhanced adsorption capability, good sensitivity values and low hysteresis.

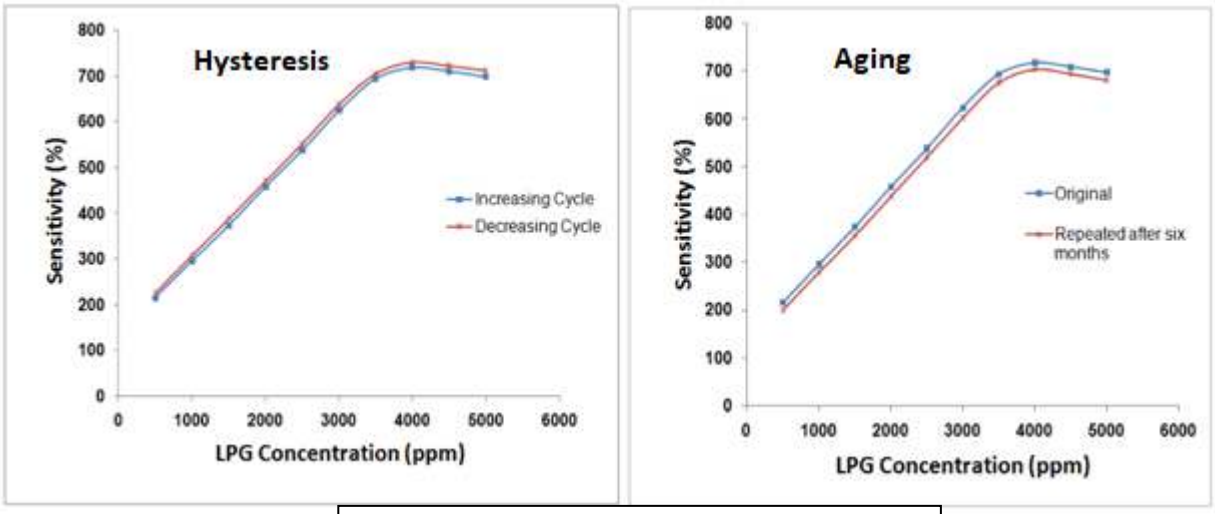

Figure 7.4 a. Hysteresis Graph b. Aging Graph

Figure 7.4(b) shows ageing effect behavior of sample CZ-7 annealed at 600°C.The effect of ageing is an important aspect in gas sensing devices based on metal oxides. After the study of gas sensing properties, sensing elements were kept in laboratory environment and the characteristics of gas sensing were regularly monitored. For analysing the effect of ageing, sensing properties of these elements were examined again in the gas control chamber after six months and variation of resistance with change in gas concentrationwas recorded. Variation of resistance of all the sensing elements with change in gas concentration after six months was analyzed. For all the sensing elements annealed at 600°C, values were generally repeatable within ±5.00% in the 500 ppm to 5000 ppmrange after six months. All the sensing elements showed significantly less ageing effect in their performance for all the annealing temperatures considered. In gas sensors ageing mechanisms may be due either to prolonged exposure of surface to atmosphere, adsorption of contaminants, loss of surface ions, or annealing to a less reactive structure, etc. The sensing elements of both undopedZnO and Cu-doped ZnO thin films showed significantly less ageing effects in their performance for all the annealing temperatures considered.These sensors give good performance up to 8-10 months but best up to 6 months that we have reported.

As the annealing temperature increases the value of response/recovery time decreases i.e., the response and recovery are getting faster with increase in annealing temperature. Response/recovery time for the sensing element CZ-0 (undoped ZnO) for the annealing temperatures 300°C, 400°C, 500°C and 600°C are 72/80, 58/67, 46/55 and 32/41 seconds respectively. Response/recovery time for the sensing element CZ-7 for the annealing temperatures 300°C, 400°C, 500°C and 600°C are 41/49, 30/36, 20/27 and 8/13seconds respectively. Thus, Cu-doped ZnO thin films gave better response and recovery time compared to the sensing element of undopedZnO. Desorption of gas molecules is a slow process; therefore, the recovery time is greater than the response time.

TABLE 7.1 Sensitivity of Samples of undoped ZnO

Annealing Temperature	**Sensitivity (%) (UndopedZnO)**		
	a	**b**	**c**
300 ºC	398	415	380
400 ºC	436	453	419
500 ºC	469	484	454
600 ºC	492	508	475
[a]Increasing cycle; [b]Decreasing cycle; [c]Increasing cycle after six months			

TABLE 7.2 Sensitivity of Samples (%)

Annealing Temp. (ºC)	Sample (CZ-1)			Sample (CZ-3)			Sample (CZ-5)			Sample (CZ-7)			Sample (CZ-8)		
	a	b	c	a	b	c	a	b	c	a	b	c	a	b	c
300 ºC	358	370	345	418	432	405	476	490	462	547	562	535	520	534	506
400 ºC	416	432	402	482	498	468	540	554	525	612	625	598	582	595	567
500 ºC	475	488	460	540	556	525	598	615	584	668	682	653	636	650	622
600 ºC	528	542	512	592	605	578	649	664	634	718	730	704	686	701	670

[a]Increasing cycle; [b]Decreasing cycle; [c]Increasing cycle after six months

References

1. Morawska, Z. Ristovski, E. R. Jayaratne, D. U. Keogh and X. Ling, "Ambient nano and ultrafine particles from motor vehicle emissions: Characteristics, ambient processing and implications on human exposure", Atmospheric Environment 42, 8113-8138 (2008).
2. S. Pizzini, N. Butta, D. Narducci, M. Palladina, "Preparation and electrical properties of undoped zinc oxide films by CVD", J. Electrochem. Society 136, 1945-1948 (1998).
3. H. W. Ryu, B. S. Park, A. A. Sheikh, W. S. Lee, K. J. Hong, Y. J. Seo, D. C. Shin, J. S. Park and G. P. Choi, "Enhanced toluene sensing characteristics of TiO2-doped flower like ZnO Nanostructures", Sensors and Actuators B96, 717-722 (2003).
4. Sergiu T. Shishiyanu, Teodor S. Shishiyanu and Oleg I. Lupan,"Sensing characteristics of tin-doped ZnO thin films as NO2 gas sensor", Sensors and Actuators B107, 379-386 (2005).
5. Can Li, Shunping Zhang, Mulin Hu and ChangeshengXie, "Growthzinc oxide nano rods obtained by hydrothermal synthesisand chemical vapor deposition", Sensors and Actuators B153, 415-420 (2011).
6. M. C. Carotta, A. Cervi and V. Di. Natale, "Preparation and Ethanol Sensing Properties of ZnO Nanoparticles via a Novel Sol-Gel Method", Sensors and Actuators B137, 164-169 (2009).
7. M. Hubner, N. Barsan and U. Weimar, "Nanoscale SnO2Hollow Spheres and Their Application as a Gas-Sensing Material", Sensors and Actuators B 151, 103-106 (2010).
8. M. Hubner, D. Koziej, M. Bauer and M. D. Rossell, "The Structure and Behavior of Platinum in SnO2-Based Sensors under Working Conditions", Chemie-International Edition50, 2841-2844 (2011).
9. Z. A. Ansari, Taegyung G. Ko, and Jae-Hee Oh, "CO-sensing properties of In2O3-doped SnO2thick-film sensors: effect of doping concentration and grain size", IEEE Sensor Journal5, 817-824 (2005).
10. G. Neri, A. Bonavita, G. Rizzo, S. Galvagno, N. Pinna, M. Niederberger, S. Capone and P. Siciliano, "Effect of the chemical composition on the sensing properties of In2O3–SnO2 nanoparticles synthesized by a nonaqueous method", Sensor and Actuators B122, 564-571 (2007).
11. M. D. Antonik, J. E. Schneider, E. L. Wittman, K. Snow, J. F. Vetelino and R. J. Lad, "Microstructural effect of WO3 gas sensing films", Thin Solid Films 256, 247-252 (1995).
12. V. Khatko, E. Llobet, X. Vilanova, J. Brezmes, J. Hubalek, K. Malysz and X. Correig, "Gas sensing properties of nanoparticle indium-doped WO3 thick films", Sensor and Actuators B45, 111-112 (2005).
13. W. Belkacem, A. Labidi, J. Guerin, N. Mliki and K. Aguir, "Cobalt nanograins effect on the ozone detection by WO3 sensors", Sensor and Actuators B 132, 196-201 (2008).
14. S. Basu and A. Dutta, "Modified heterojunction based on zinc oxide thin film for hydrogen gas-sensor application", Sensor and Actuators B22, 83–87 (1994).
15. G. Sberveglieri, P. Nelli, S. Groppelli, F. Quaranta, A. Valentini and L. Vasanelli, "Oxygen gas sensing characteristics at ambient pressure of undoped and lithium-doped ZnO sputtered thin filmd", Materials Science and Engineering: B 7, 63–68 (1990).
16. Uwe Lampe and Jörg Müller, "Thin-film oxygen sensors made of reactively sputtered ZnO", Sensor and Actuators B18, 269–284 (1989).
17. E. Traversa and A. Bearzotti, "A novel humidity-detection mechanism for ZnO dense pellets", Sensor and Actuators B23, 181–186 (1995).
18. M. Hjiri, L. El Mir, S. G. Leonardi, N. Donato and G.Neri, "CO and NO2Selective Monitoring by ZnO-Based Sensors", J. Nanomaterial3 357–369 (2013).
19. C. Baratto, G. Sberveglieri, A. Onischuk, B. Caruso and S. di Stasio, "Low temperature selective NO2 sensors by nanostructured fibres of ZnO", Sensor and Actuators B100, 261–265 (2004).
20. S. C. Yeow, W. L. Ong, A. S. W. Wong and G. W. Ho, "Template-free synthesis and gas sensing properties of well-controlled porous tin oxide nanospheres", Sensor and Actuators B143, 295–301 (2009).
21. Horst Bauer, Automotive Handbook (4^{th}ed.) Stuttgart, (1996).
22. K. L. Chopra, S Major, and D. K Pandya, "Transparent conductors—A status review", Thin Solid Films 102, 1–46 (1983).

23. M. C. Horrillo, J. Gutier´rez, L. Ares, J. I. Robla, I. Sayago and J. Getino, "The influence of the tin-oxide deposition technique on the sensitivity to CO", Sensors and Actuators B25, 507–511 (1995).
24. G. Sberveglieri, "Recent development in semiconducting thin film gas sensors", Sensors and Actuators B 23, 103–109 (1995).
25. A. Jones, T. A. Jones, B. Mann and J. G. Firth, "Theeffect of physical from the oxide on the conductivity changes produced by CH4, CO and H2O on ZnO" Sensors &Actuators B6, 75–88 (1984).
26. D. Kohl, "Surface processes in the detection of reducing gases with SnO2-based devices", Sensors &Actuators B 18, 71-113 (1989).
27. S. D. Charpe, F. C. Raghuwanshi, "Synthesis, Structural and Gas Sensing Properties of Pure Zinc Oxide Nano Thick film", Journal of Electron Devices 21, 1854-1861 (2015) 1861.
28. Arindam Ghosh, Ramphal Sharma, Anil Ghule, Vidya S. Taur, Rajesh A. Joshi, Dipalee J. Desale, Yuvraj G. Gudage, K. M. Jadhav and Sung-Hwan Han, "Low temperature LPG sensing properties of wet chemically grown zincoxide nanoparticle thin film", Sensors and Actuators B: Chemical 146, 69-74 (2010).
29. AarthySivapunniyam, NitiWiromrat, MyoTayZarMyint and Joydeep Dutta, "High-performance liquefied petroleum gas sensing based on nanostructures of zinc oxide and zinc stannate", Sensors and Actuators B: Chemical157 232-239 (2011).
30. P. P. Sahay and R. K. Nath, "Al-doped zinc oxide thin films for liquid petroleum gas (LPG) sensors", Sensors and Actuators B 133, 222–227 (2008).
31. L. A. Patil , A. R. Bari, M. D. Shinde and Vinita Deo, "Ultrasonically prepared nanocrystallineZnO thin films for highly sensitive LPG sensing", Sensors and Actuators B: Chemical 149, 79-86 (2010).
32. Tanushree Sen, Navinchandra G. Shimpi, Satyendra Mishra and Ramphal Sharma,"Polyaniline/γ-Fe2O3nanocomposite for room temperature LPG sensing", Sensors and Actuators B: Chemical 190, 120-126 (2014).
33. K. V. Gurav, P. R. Deshmukh and C. D. Lokhande, "LPG sensing properties of Pdsensitized vertically aligned ZnOnanorods", Sensors and Actuators B: Chemical 151, 365-369 (2011).
34. V. R. Shinde, T. P. Gujar and C. D. Lokhande, "LPG sensing properties of ZnO films prepared by spray pyrolysis method: Effect of molarity of precursor solution", Sensors and Actuators B: Chemical 120, 551-559 (2007).
35. O. Wurzinger and G. Reinhardt, "CO-Sensing Properties of Doped SnO2 Sensors in H2-Rich Gases",*Sensors and Actuators B*, Vol. 103, No. 1-2, 2004, pp. 104-110.
36. C. C. Chai, J. Peng and B. P. Yan, "Preparation and Gas-Sensing Properties of αFe2O3thin Films",*Journal of Electronic Materials*, Vol. 24, No. 7, 1995, pp. 799-804.
37. J. H. Yu and G. M. Choi, "Selective CO Gas Detection of CuO- and ZnO Doped SnO2 Gas Sensor",*Sensors and Actuators B*, Vol. 75 No. 1-2, 2001, pp. 56-61.
38. S. T. Shishiyanu, T. S. Shishiyanu and O. I. Lupan, "Novel NO2 Gas Sensor Based on Cuprous Oxide Thin Films",*Sensors and Actuators B*, Vol. 113 No. 1, 2006, pp. 468-476.
39. A. Chaturvedi, V. N. Mishra, R. Dwivedi and S. K. Sri-vastava, "Selectivity and Sensitivity Studies on Plasma Treated Thick Film Tin Oxide Gas Sensors",*Microelec-tronics Journal*, Vol. 31 No. 4, 2000, pp. 283-290.
40. Shishiyanu, S.T., Shishiyanu, T.S. andLupan, O.I.,"Sensing characteristics of tin-doped ZnO thin films as NO2 gas sensor", Sens. Actuators B Chem., 107, 379–386, 2005.
41. Musat, V., Rego, A.M., Monteiro, R. and Fortunato, E., "Microstructure and gas-sensing properties of sol–gel ZnO", Thin Solid Films, 516, 1512–1515, 2008.
42. Shin, M.C., Lay, G.T., Wei, H.L., Yen, H.S.and Min, H.H., "ZnO:Al thin film gas sensor for detection of ethanol vapor", Sensors, 6, 1420–1427, 2006.
43. Shinde, V.R., Gujar, T.P. andLokhande, C.D., "Enhanced response of porous ZnOnanobeads towards LPG: Effect of Pd sensitization", Sens. Actuators B Chem., 123, 701–706, 2007.
44. Wei, S., Yu, Y. and Zhou, M, "Co gas sensing of Pd-doped ZnOnanofibres synthesized by electrospinning method", Mater. Lett., 64, 2284–2286, 2010.
45. Yu, P., Wang, J., Du, H., Yao, P., Hao, Y. and Li, X., "Y-doped ZnOnanorods by hydrothermal method and their acetone gas sensitivity", J. Nanomater., 2013, 1–6, 2013.

46. Chow, L., Lupan, O., Chai, G., Khallaf, H., Ono, L.K., Roldan-Cuenya, B., Tiginyanu, I.M., Ursaki, V.V., Sontea, V. and Schulte, A, "Synthesis and characterization of Cu-doped ZnO one-dimensional structures for miniaturized sensor applications with faster response", Sens. Actuators A Phys., 189, 399–408, 2013.
47. N. K. Pandey, Karunesh Tiwari, and Akash Roy, "Moisture sensing application of Cu_2O doped ZnOnanocomposites", IEEE Sensors Journal, 11 (9), 2142, 2011.
48. Suneet Kumar Misra, Narendra Kumar Pandey, VandnaShakya, and Akash Roy, "Application of Undoped and Al2O3-doped ZnO Nanomaterials as Solid-State Humidity Sensor and its Characterization Studies", IEEE Sensors Journal, vol. 15, issue. 6, p. 3582, 2015.
49. Suneet Kumar Misraand Narendra Kumar Pandey, "Analysis on Activation Energy and Humidity Sensing Application of Nanostructured SnO_2-doped ZnO Material",Sens. Actuators A Phys. 249, 8–14, 2016.
50. Suneet Kumar Misraand Narendra Kumar Pandey, "Study of Activation Energy and Humidity Sensing Application of Nanostructured Cu-doped ZnO Thin Films", Journal of Materials Research, vol. 31, issue 20, pp. 3214-3222, 2016.
51. Shewale, P.S., Patil, V.B., Shin, S.W., Kim, J.H. and Uplane, M.D., "H2S gas sensing properties of nanocrystalline Cu-doped ZnO thin films prepared by advanced spray pyrolysis", Sens. Actuators B Chem. 186, 226–234, 2013.
52. G. Martinelli, M. C. Carotta, M. Ferroni, Y. Sadaoka and E. Traversa, "Screen-Printed Perovskite-Type Thick Films as Gas Sensors for Environmental Monitoring",Sensors and Actuators B: Chemical, Vol. 55, No. 2-3, 1999, pp. 99-110.
53. Serrini, P., Briois, V., Horrillo, M.C., Traverse, A. and Manes, L., "Chemical composition and crystalline structure of SnO2 thin films used as gas sensors", Thin Solid Films, 304, 113–122, 1997.
54. Gong, H., Hu, J.Q., Wang, J.H., Ong, C.H. and Zhu, F.R., "Nano-crystalline Cu-doped ZnO thin film gas sensor for CO",Sensors and Actuators B: Chemical, 115, 247–251, 2006.

CHAPTER VIII

Nanostructured Zinc Oxide Prepared through Solid State Reaction Route as Gas Sensor

In this chapter we report the characterization and Gas sensing studies of ZnO nanoparticles and its application as LPG sensor. The pellet samples have been made under a pressure of 390 M Pascal at room temperature. LPG sensing properties of each pellet has been investigated. The surface and gross structural characterization of the sensing element have been carried out by scanning electron microscopy (SEM) and powder x-ray diffraction (PXRD) techniques respectively

8.1 Fabrication of Nanomaterial Samples

The starting material was ZnO (MERC, India Ltd, 99.99% pure) and glass powder. Glass powder (Ethyl Cellulose) has been used as binder to increase the strength of the sample. ZnO with 5 weight % of glass powder (binder) were mixed uniformly and made fine. The resultant powder was pressed into pellet shape by uniaxially applying pressure of 390 MPa. These Pellets were annealed in electric muffle furnace at different temperatures 300°C (sample Zn-3), 500°C (sample Zn-5) and 700°C (sample Zn-7) for four hours and cooled to room temperature.

8.2 Results and Discussion

Figure 8.1 is the graphs between variations in resistance (R_g) with the variation of pressure for different exposure time for sample pure ZnO annealed at temperature 700°C. In this graph

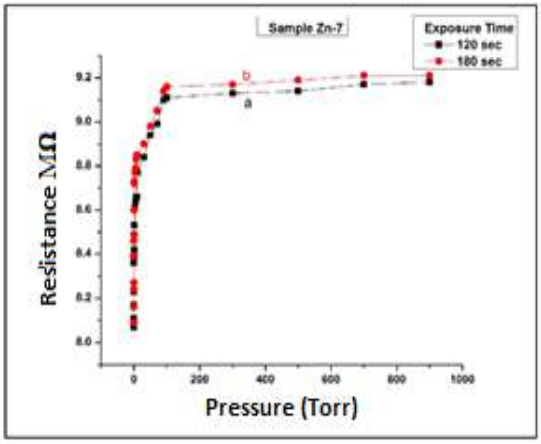

Figure 8.1 Resistance (Rg) Vs pressure for different exposure time for (Zn-7).

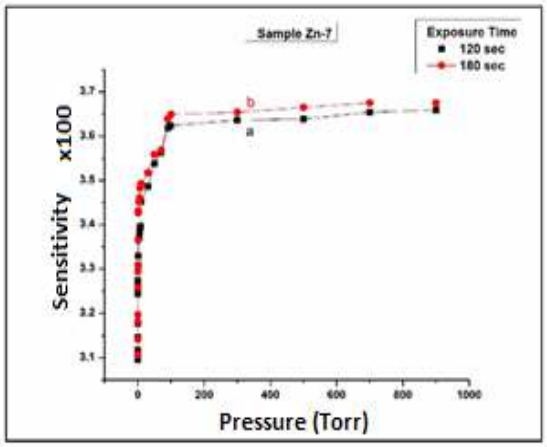

Figure 8.2 Sensitivity Vs pressure for different exposure time for Zn-7.

curve 'a' is for exposure time of 120 sec and curve 'b' for exposure time of 180 sec. Curve 'a' of this graph show that there is a continuous increase in resistance from 8.07 M**Ω** to 9.18 M**Ω**, curve 'b' also show increase in resist**a**nce from 8.09 M**Ω** to 9.21 M**Ω** with better results.Figure 8.2 is the graphs between variations in sensitivity with the variations of pressure for different exposure time for sample pure ZnO annealed at temperature 700°C. In this graph curve 'a' is for exposure time of

120 sec and curve ‘b’ for exposure time of 180 sec. Curve ‘b’ of this figure show slight better sensitivity in compare to curve ‘a’. The average sensitivity for sample Zn-7 exposure time of 120 sec is 339, while for exposure time of 180 sec is 344.

Figure 8.3 is the graphs between variations in resistance (R_g) with the variations ofpressure for all the samples of pure ZnO for exposure Time (120 sec). For exposure time of 120 sec the variation in resistance with the variation of pressure for all the samples of Pure ZnO (i.e Zn-3, Zn-5 and Zn-7) show similar trends. Curve ‘a’ of figure 8.3 shows a continuous increase in resistance, while curve ‘b’ and ‘c’ of same figure also show increase in resistance.

Figure 8.4 is the graphs between variations in resistance (R_g) with the variation ofpressure for all the samples of pure ZnO for exposure time (180 sec). For exposure time of 180 sec the variations in resistance with the variation of pressure for all the samples of PureZnO (i.e Zn-3, Zn-5 and Zn-7) show similar trends. A slight increase in resistance has been found as a function of pressure. Curve

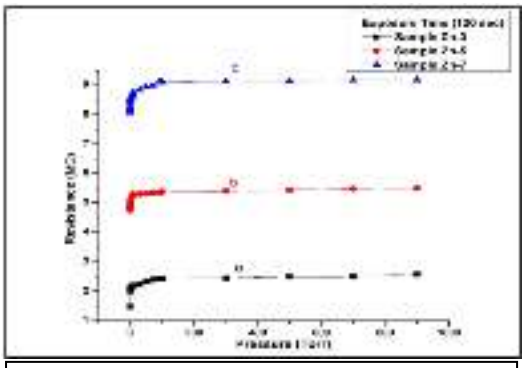

Figure 8.3 Resistance Vs Pressure for pure ZnO for exposure time (120 sec).

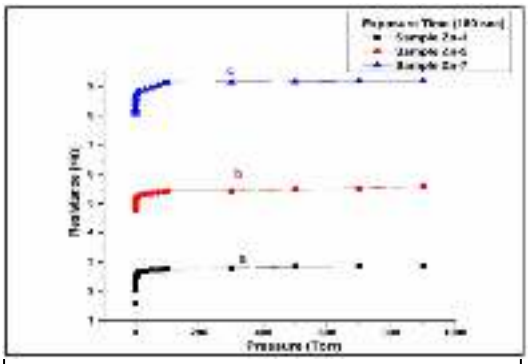

Figure 8.4 Resistance Vs pressure for pure ZnO for exposure time (180 sec).

‘a’ of figure 8.4 shows a continuous increase in resistance, while curve ‘b’ and ‘c’ of same figure also show increase in resistance.

Figure 8.5 is the graphs between variation in resistance (R_g) with the variations ofpressure for sample (Zn-7) for exposure time of 180 sec. In this graph curve ‘a’ is for original cycle and curve ‘c’ is for repeated cycle after one month corresponding to the same experiment. Ageing effect for the sensing material (Zn-7) for exposure time of 180 sec was investigated and found that there is a slight decrease in value of resistance with respect to pressure after one month. The average sensitivity (S) for different exposure time for pure ZnO samples (Zn-3, Zn-5 and Zn-7) have been calculated and are given in Table 8.1.

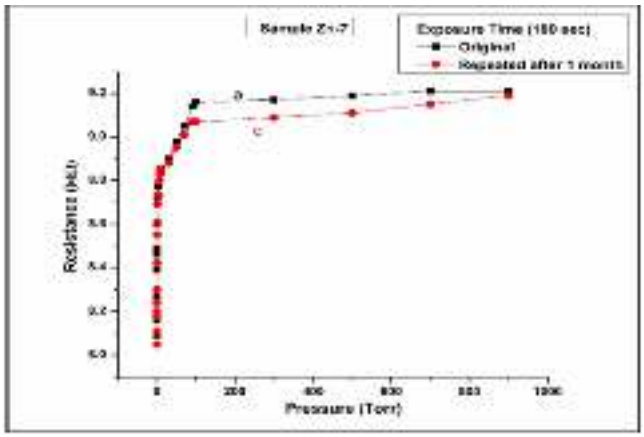

Figure 8.5 Resistance Vs Pressure for Zn-7 for exposure time 180 sec; a. original cycle and c. repeated cycle after one month.

Table 8.1 Average sensitivity for different exposure time

Samples	Average Sensitivity	
	120 sec	180 sec
Zn-3	115	145
Zn-5	213	216
Zn-7	339	343

LIST OF PUBLICATIONS

i. Moisture Sensing Studies of CuO-ZnONanocomposites, Vijaya Rajput, Narendra Kumar Pandey, **International Journal of Applied Ceramic Technology** Volume 14, Issue 1January/February **2017** pp 77–83.

ii. Study of Activation Energy and Humidity Sensing Application of Nanostructured Cu-doped ZnO Thin Films, Suneet Kumar Misra, Narendra Kumar Pandey, **Journal of Materials Research**Volume 31, Issue 20 October **2016**, pp. 3214-3222.

iii. Application of Undoped and Al_2O_3-Doped ZnO Nanomaterials as Solid-State Humidity Sensor and its Characterization Studies, Suneet Kumar Misra, Narendra Kumar Pandey, V Shakya, A Roy, **IEEE Sensors Journal** 15 (6), **2015** pp 3582-3589.

iv. Electricaland optical properties of ZnO-WO_3 nanocomposite and its application as solid state humidity sensor, **Bulletin of Materials Science**, VandnaShakya, N K Pandey, Suneet Kumar Misra, Akash Roy, Vol. 40, No. 2, pp. 253–262 April 2017.

v. Humidity Sensor Based on Synthesized WO3–SnO2 Nanocomposites, A Roy, Narendra Kumar Pandey, V Shakya, A Kumar, **Energy and Environment Focus** 2 (2), 126-132 (2013).

vi. Characterization and humidity sensing application of WO3-SnO2 nanocomposite, Narendra Kumar Pandey, V Shakya, S Mishra, **IOSR Journal of Applied Physics**, 4 (3) 10-17 2013.

vii. Analysis on activation energy and humidity sensing application of nanostructured SnO2-doped ZnO material, Suneet Kumar Misra, Narendra Kumar Pandey, **Sensors and Actuators A: Physical** 249, **2016** pp 8-14.

viii. Characterization of Nanocomposites of WO_3–SnO_2 and its Application as a Moisture Sensors, A Roy, Narendra Kumar Pandey, V Shakya, S Misra, S Singh, A Kumar, A Kumar, **Advanced Science Letters** 22 (1), **2016** pp 188-192.

ix. Application of V_2O_5-ZnO Nanocomposite for Humidity Sensing Studies, **Int. Journal of Materials Science and Applications**, 6(3) 119-125 2017.

Papers Presented in International/National Conferences/Seminars

x. Suneet Kumar Misra, Narendra Kumar Pandey, Investigation of Electrical Properties, Activation Energy and Humidity/Gas Sensing Studies of Synthesized Al Doped ZnO Nanomaterials , Proc. 6th International Conference **2014** Nanocon, Nov 5-7, 2014, Tanger Ltd., The Czech Society for New Materials and Technologies, Brno, Czech Republic, EU, B-16, p.55.

xi. Anupam Kumar Tripathi, Narendra Kumar Pandey, VidhuTripathi, Karunesh Tiwari, Humidity Sensing Studies of Nanoporous Zinc Tungstate Ceramic Sensor, P-42, p.140, 22nd International Conference of International Academy Of Physical Sciences (CONIAPS XXII) on Emerging Trends in Physical Sciences, April 13-15, 2018 Organized By Faculty Of Science, Dr. Ram Manohar LohiaAvadh University, Faizabad-224001, U.P., INDIA,

xii. Karunesh Tiwari, Narendra Kumar Pandey, Humidity Sensor Based on Zinc Oxide-Zinc Tungstate Nanocomposite,, P-20, p.129, 22nd International Conference of International Academy Of Physical Sciences (CONIAPS XXII) on Emerging Trends in Physical

Sciences, April 13-15, 2018 Organized By Faculty Of Science, Dr. Ram Manohar LohiaAvadh University, Faizabad-224001, U.P., INDIA,

xiii. Narendra Kumar Pandey, Metal Oxide Nanomaterials for Humidity/Gas Sensing Studies, 22nd International Conference of International Academy Of Physical Sciences (CONIAPS XXII) on Emerging Trends in Physical Sciences, Dr. RML Avadh University, Faizabad-224001, U.P., April 13-15, 2018.

xiv. Akash Roy, Narendra Kumar Pandey, VandnaShakya, SuneetMisra, Sanchita Singh, Anoop Kumar, Alok Kumar, Proceedingsof The First International Conference on Emerging Materials: Characterization & Application "Characterization of Nanocomposites of WO_3-SnO_2 and its Application as a Moisture Sensor" organized by CGCRI, Kolkata, 4-6 **Dec, 2014**, page-87.

xv. Narendra Kumar Pandey, International Symposium on advances in Biological and Materials Science (ISABMS-**2014**), Department of Physics, University of Lucknow

xvi. Narendra Kumar Pandey, Akash Roy, K. Tiwari, Comparative Studies of Moisture Sensing Application of Ag- and SnO_2 Doped WO_3, OP-79, Proc. Int. Conf. on Nanoscience and Nanotechnology, BabasahebBhimraoAmbedkarUniv, Lucknow, India, pp.78, 2013.

xvii. Anoop Kumar Gautam, Abhishek Panwar, Sanchita Singh, N.K. Pandey, Humidity Sensing Investigations of Nanostructured Pure and Silver Doped Titanium Oxide, pp-30, Proc. Int. Conf. on Nanoscience and Nanotechnology, BabasahebBhimraoAmbedkarUniv, Lucknow, India, pp.119, 2013.

xviii. Narendra Kumar Pandey, Suneet Kumar Misra, VandanaShakya, Alok Kumar, Characterization and Humidity Sensing Studies of Al_2O_3 Doped ZnO nanomaterial, PP-172, Proc. Int. Conf. on Nanoscience and Nanotechnology, BabasahebBhimraoAmbedkarUniv, Lucknow, India, pp.197, 2013.

xix. Narendra Kumar Pandey, International Seminar on Advances in Bio- &Nano- Materials, Dept of Physics, University of Lucknow, 2013.

xx. Narendra Kumar Pandey, Paper presented at International Symposium on advances in Biological and Materials Science (ISABMS-2014), Department of Physics, University of Lucknow

xxi. Narendra Kumar Pandey, Akash Roy, K. Tiwari, Comparative Studies of Moisture Sensing Application of Ag- and SnO_2 Doped WO_3, OP-79, Proc. Int. Conf. on Nanoscience and Nanotechnology, BabasahebBhimraoAmbedkarUniv, Lucknow, India, pp.78, 2013.

xxii. Anoop Kumar Gautam, Abhishek Panwar, Sanchita Singh, N.K. Pandey, Humidity Sensing Investigations of Nanostructured Pure and Silver Doped Titanium Oxide, PP-30, Proc. Int. Conf. on Nanoscience and Nanotechnology, BabasahebBhimraoAmbedkarUniv, Lucknow, India, pp.119, 2013.

xxiii. Suneet Kumar Misra, Narendra Kumar Pandey, VandnaShakya, Akash Roy, Study of Characterization and Humidity Sensing Application of Al_2O_3 Doped ZnO Nanomaterials, Science Congress, 3-7 January, 2015.

xxiv. Pandey N K, Metal Oxide Humidity Sensors, International e-journal Manthan, Vol 11, pp.44-46, June 2010 (ISSN No.974-6331).

xxv. Narendra Kumar Pandey, Sunnet Kumar Misra, VandanaShakya, Alok Kumar, Aluminum Oxide Doped Zinc Oxide nanomaterials as Moisture Sensor, PP-50, Proc. 7th National Conf. on Thermophysical Properties (NCTP), Dept of Physics, Christ Church College, Kanpur, India, pp.138-**39, 2013.**

Invited Talks Delivered

xxvi. Invited Talk on metal oxides as generic humidity and gas sensor, National conference on Recent Advances and Innovations in Chemical and Materials Science, JNPG College, Lucknow, 23-24 February, 2017.

xxvii. Invited Talk on Humidity Sensors based on Metal Oxide Nanomaterial, Proc. International Conf. on Nanoscience and Nanotechnology, BabasahebBhimraoAmbedkarUniv, Lucknow, India, 2013.

xxviii. Invite Talk on Metal Oxide Humidity Sensor, 7th National Conf. on Thermophysical Properties (NCTP), Dept of Physics, Christ Church College, Kanpur, India, 2013.

xxix. Invited talk at B.R. Ambedkar University, Muzaffarpur, Bihar, 13 November, 2013, Nanotechnology: Basics and Future Prospects.

Ph.D. Work Completed out of the project: 05